JOURNAL OF PETROLOGY

Journal of Petrology, 2018, 1–24
doi: 10.1093/petrology/egy081
Advance Access Publication Date: 13 August 2018
Original Article

OXFORD

Lateral Variability in the Upper Main Zone, Bushveld Complex, owing to Directional Magma Recharge and Emplacement from North to South

Jacob B. Setera * and Jill A. VanTongeren

Department of Earth and Planetary Sciences, Rutgers University, Piscataway, NJ 08854, USA

*Corresponding author. E-mail: jacob.setera@rutgers.edu

Received September 21, 2017; Accepted August 1, 2018

ABSTRACT

Recharge and magma mixing into shallow crustal reservoirs is a critical parameter in understanding magma diversity and predicting volcanic activity and hazards. Direct observation of magma mixing within the crust, however, is impossible. The solidified remnants of large magma chambers in layered mafic intrusions are therefore some of the most important natural laboratories for measuring and understanding past magma chamber dynamics. Here we provide *in situ* major and trace element compositions of all major mineral phases throughout a single stratigraphic section of a well-defined magma recharge interval in the ~2·06 Ga Bushveld Complex layered intrusion of South Africa. This section, the Roossenekal Traverse, is located ~75 km south of a previously documented section of the same stratigraphy, the Leolo Mountain Traverse. Despite their distance, the two profiles show remarkably similar thicknesses and compositional variations; however, both resident and incoming magmas recorded in the Roossenekal Traverse are slightly more compositionally evolved. We show that the lateral compositional variability is a direct result of the locus of magma recharge originating in the north, near the Thabazimbi–Murchison Lineament. New primitive magma was emplaced in the north, mixed with more evolved magma towards the south, and fractionated as it filled the magma chamber progressively to the south.

Key words: Bushveld Complex; lateral variation; magma mixing; Main Zone; Pyroxenite Marker; UUMZ

INTRODUCTION

The solidified remnants of large magma chambers in layered mafic intrusions remain some of the most important natural laboratories for measuring and understanding past magma mixing and recharge events. Evidence in support of magma mixing and recharge in the cumulates of layered intrusions can be identified by major shifts in whole-rock isotopic composition as well as reversals to more primitive major and trace element compositions with increasing height in the stratigraphic sequence (e.g. VanTongeren, 2018).

One layered intrusion in particular, the Rustenberg Layered Suite (RLS) of the Bushveld Complex, shows clear evidence of discrete magma mixing and recharge events throughout its stratigraphy. The ~2·06 Ga RLS is ~8–9 km thick, spans ~450 km east–west, 150–200 km north–south (SACS, 1980) and occurs in four distinct limbs (Northern, Western, Eastern and the Southern Bethal lobe; Fig. 1). The mafic–ultramafic magmas of the RLS were emplaced in at least four major injections (Eales, 2002). The last of these major injections occurred near the top of the Main Zone of the RLS, below the Pyroxenite Marker (Fig. 2). Evidence for a new magma injection at this level comes from clear reversals to more primitive major and trace element chemistry as well as distinctly lower whole-rock initial $^{87}Sr/^{86}Sr$ compositions (Sharpe, 1985; Kruger *et al.*, 1987; Cawthorn *et al.*, 1991; VanTongeren & Mathez,

© The Author(s) 2018. Published by Oxford University Press. All rights reserved. For permissions, please e-mail: journals.permissions@oup.com

Downloaded from https://academic.oup.com/petrology/advance-article-abstract/doi/10.1093/petrology/egy081/5073045 by Rutgers University Libraries/Technical Services user on 02 October 2018

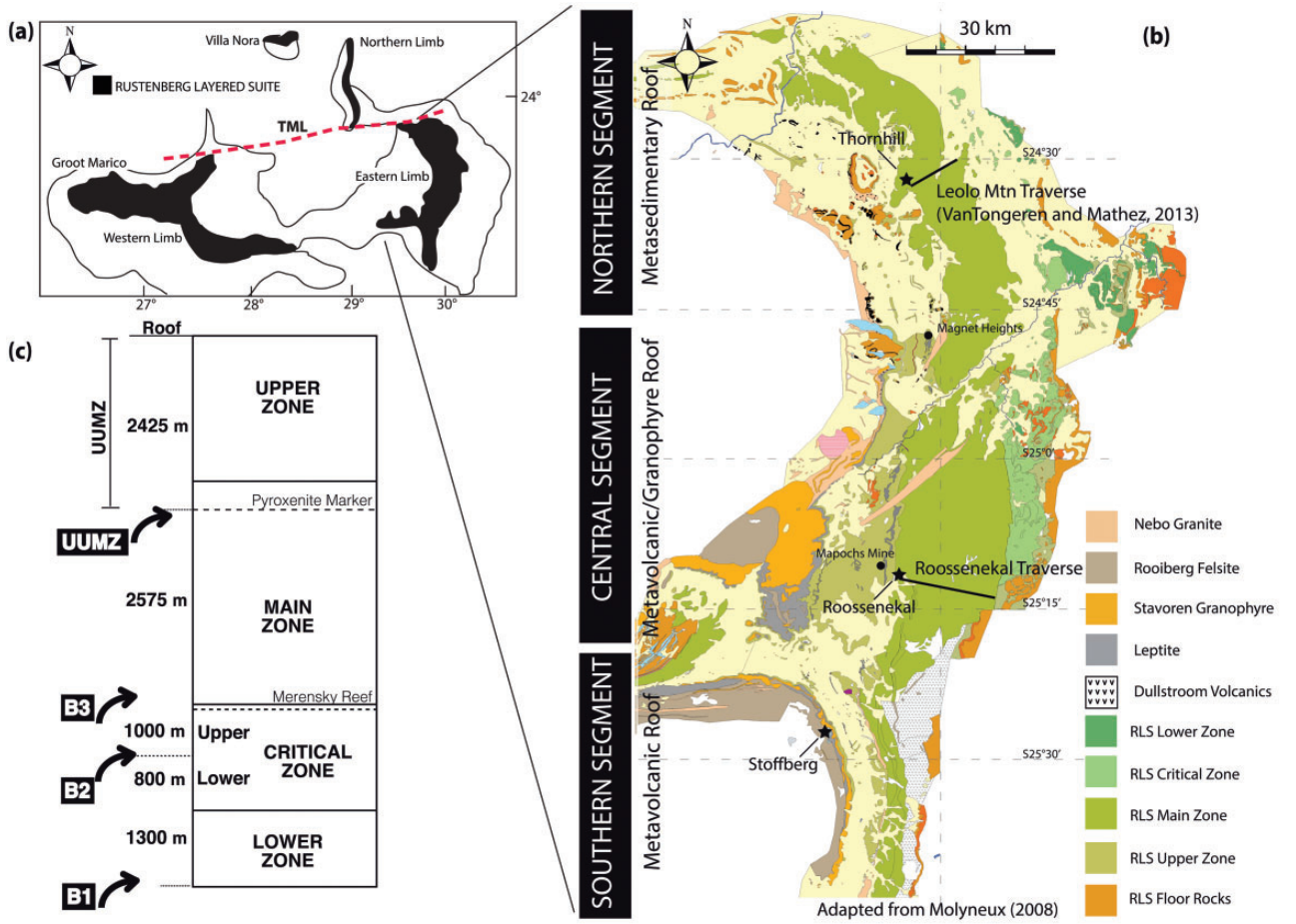

Fig. 1. (a) Generalized map of the Bushveld Complex and the predominantly mafic and ultramafic Rustenburg Layered Suite (RLS), showing the approximate location of the Thabazimbi–Murchison Lineament (TML), the likely locus for magma injection below the Pyroxenite Marker. (b) Geological map of the eastern Bushveld Complex adapted from VanTongeren & Mathez (2015). Continuous black lines indicate the two traverses that are the focus on this study. (c) Generalized stratigraphic column of the Rustenburg Layered Suite of the Eastern Limb of the Bushveld Complex, adapted from VanTongeren *et al.* (2010). Main Zone and UUMZ thicknesses at Roossenekal are discussed in the text, whereas thicknesses for the Critical and Lower Zones are estimates from Molyneux (2008).

2013). The stratigraphic interval, in which compositions become progressively more primitive upwards through the stratigraphy prior to the Pyroxenite Marker, was investigated by VanTongeren & Mathez (2013) in the Eastern Limb near the Leolo Mountains (Fig. 1) and is defined as the 'Zone of Magma Mixing' (Fig. 2).

Many scenarios involving the input of new primitive magma have been described to explain the compositional reversal within cumulus minerals below the Pyroxenite Marker. Based on higher Al_2O_3 contents of pyroxenes immediately above the Pyroxenite Marker in the Western Limb, Cawthorn *et al.* (1991) proposed that the incoming magma was denser than the resident magma and was emplaced into a stratified, poorly mixed, resident magma chamber. However, the uniformity of the whole-rock Sr isotopic compositions from the Pyroxenite Marker to the roof (e.g. Sharpe, 1985; Kruger *et al.*, 1987), and the clear trends in *in situ* major and trace element compositions of plagioclase and pyroxenes, led VanTongeren & Mathez (2013) to conclude that the new magma was emplaced in multiple small batches into a homogeneous resident magma body. Rapid mixing between incoming and resident magma allowed for homogenization of the two magmas and partial crystallization between each pulse.

With the exception of a recent study looking at lateral changes in plagioclase An content at the Pyroxenite Marker (e.g. Cawthorn *et al.*, 2016), the majority of studies attempting to elucidate the nature of this magma recharge event (i.e. compositions and volume of incoming magma), focus on individual boreholes or single stratigraphic sections and do not investigate potential lateral variation within the magma chamber. Incorporating lateral variations into previous findings regarding magma chamber dynamics is vital, particularly in the case of the RLS because of its immense size.

The goal of this work is to use *in situ* major and trace element analyses to investigate the lateral variation in the magma chamber during the final recharge event into the RLS near the level of the Pyroxenite Marker.

Downloaded from https://academic.oup.com/petrology/advance-article-abstract/doi/10.1093/petrology/egy081/5073045 by Rutgers University Libraries/Technical Services user on 02 October 2018

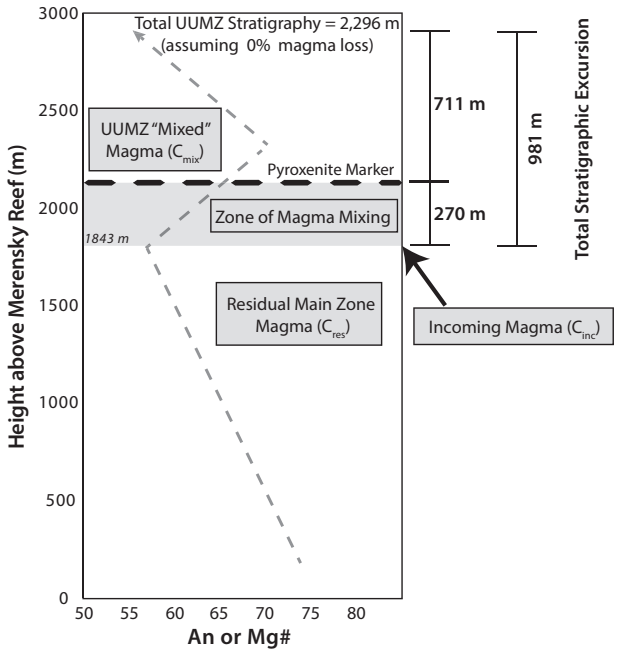

Fig. 2. Illustration of the mixing interval below the Pyroxenite Marker, adapted from VanTongeren & Mathez (2013). Stratigraphic thicknesses are for the Roossenekal Traverse and are discussed in the text. Grey dashed line through the stratigraphy shows general change in plagioclase An content and pyroxene Mg# through the stratigraphy.

GEOLOGICAL AND STRATIGRAPHIC SETTING

The RLS was intruded around 2·06 Ga (Buick *et al.*, 2001; Scoates & Friedman, 2008; Olsson *et al.*, 2010; Scoates & Wall, 2015; Zeh *et al.*, 2015; Mungall *et al.*, 2016) into Neoarchean to Paleoproterozoic Transvaal Supergroup sediments (Eriksson & Altermann, 1998) within the central NE portion of the Kaapvaal craton. The layered sequence crops out predominantly in the Eastern and Western limbs, which dip gently toward each other and appear to connect at depth (Cawthorn & Webb, 2001; Webb *et al.*, 2004) (Fig. 1). The predominantly mafic and ultramafic unit of the Bushveld Complex, the Rustenburg Layered Suite (RLS), is stratigraphically subdivided (SACS, 1980) into the Lower, Critical, Main and Upper Zones based on cumulus mineral assemblages (Fig. 1). It is in the Eastern Limb that the RLS is best exposed.

The estimated thickness of the Main Zone varies considerably from north to south in the Eastern Limb. The Main Zone in the Eastern Limb of the RLS has been described to be ~2900 m in the north near the Leolo Mountains (Molyneux, 1974) to ~3940 m (von Gruenewaldt, 1973) or 2635 m (Fig. 3; this study) at Roossenekal and ~1100–1450 m at Stoffberg toward the south (Groeneveld, 1970) (Fig. 1). Some of the variability in estimates arises from ambiguity in the official boundary between the base of the Main Zone and the top of the Critical Zone (Kruger, 1990, 1991; Mitchell & Scoon, 1991). The South African Commission for Stratigraphy (SACS, 1980) positions the boundary above the Merensky Reef on top of a distinct series of anorthositic rocks containing large mottled pyroxene called the Bastard mottled anorthosite (Giant mottled anorthosite). A re-examination of the Main Zone boundaries by Kruger (1990) places the base of the Main Zone at an unconformity immediately below the Merensky Reef, where there is a distinctive change in the whole-rock strontium isotopic signature (Kruger, 1994). Above the Merensky Reef, the Main Zone consists of norite, gabbronorite and occasional anorthosite layers. Inverted pigeonite eventually replaces orthopyroxene as the Ca-poor pyroxene upwards through the stratigraphy.

The Main Zone–Upper Zone boundary is officially defined as the first appearance of cumulus magnetite (SACS, 1980). However, it is below the Pyroxenite Marker, a nearly ubiquitous ~3 m thick orthopyroxenite layer in the upper Main Zone, that the whole-rock Sr isotopic composition changes and the major element compositions of the cumulus mineral phases become more primitive (Kruger *et al.*, 1987; Cawthorn *et al.*, 1991; VanTongeren & Mathez, 2013). The change in whole-rock Sr isotopes across this boundary led Kruger *et al.* (1987) to define the geochemical boundary between the Upper Zone and Main Zone at the level of the Pyroxenite Marker. To avoid confusion with nomenclature, the stratigraphy from the Pyroxenite Marker to the roof of the intrusion, which encompasses the combined Upper Zone and Upper Main Zone, has been termed the UUMZ (Fig. 2c; VanTongeren *et al.*, 2010).

In the Eastern Limb, the Pyroxenite Marker has been traced along-strike from north to south before disappearing ~5 km south of Roossenekal. Where the Pyroxenite Marker is absent in the south, it is replaced by magnetite gabbro although still recording compositional reversals similar to those observed in the north (von Gruenewaldt, 1973; Klemm *et al.*, 1985; Cawthorn *et al.*, 2016). Owing to poor outcrop availability, the Western Limb is primarily studied via boreholes and only a single representation of the Pyroxenite Marker has been found (Cawthorn *et al.*, 1991), although compositional reversals have been recorded without the presence of the Pyroxenite Marker (Mitchell, 1990). The Pyroxenite Marker is entirely absent from boreholes and exposed outcrop in the Northern Limb. Although there are two pyroxene-rich horizons observed within a borehole from the Northern Limb, Ashwal *et al.* (2005) concluded, based on mineralogical evidence, that these are not correlated with the Pyroxenite Marker.

Previous lateral variation studies at the level of the Pyroxenite Marker

Lateral variation in the RLS magma chamber at the level of the Pyroxenite Marker was previously investigated on a small scale in a study by Klemm *et al.* (1985). Klemm *et al.* (1985) measured three profiles just south of Roossenekal spaced over ~10 km along-strike. Those researchers measured bulk plagioclase (measured on a universal stage) and orthopyroxene compositions

Downloaded from https://academic.oup.com/petrology/advance-article-abstract/doi/10.1093/petrology/egy081/5073045 by Rutgers University Libraries/Technical Services user on 02 October 2018

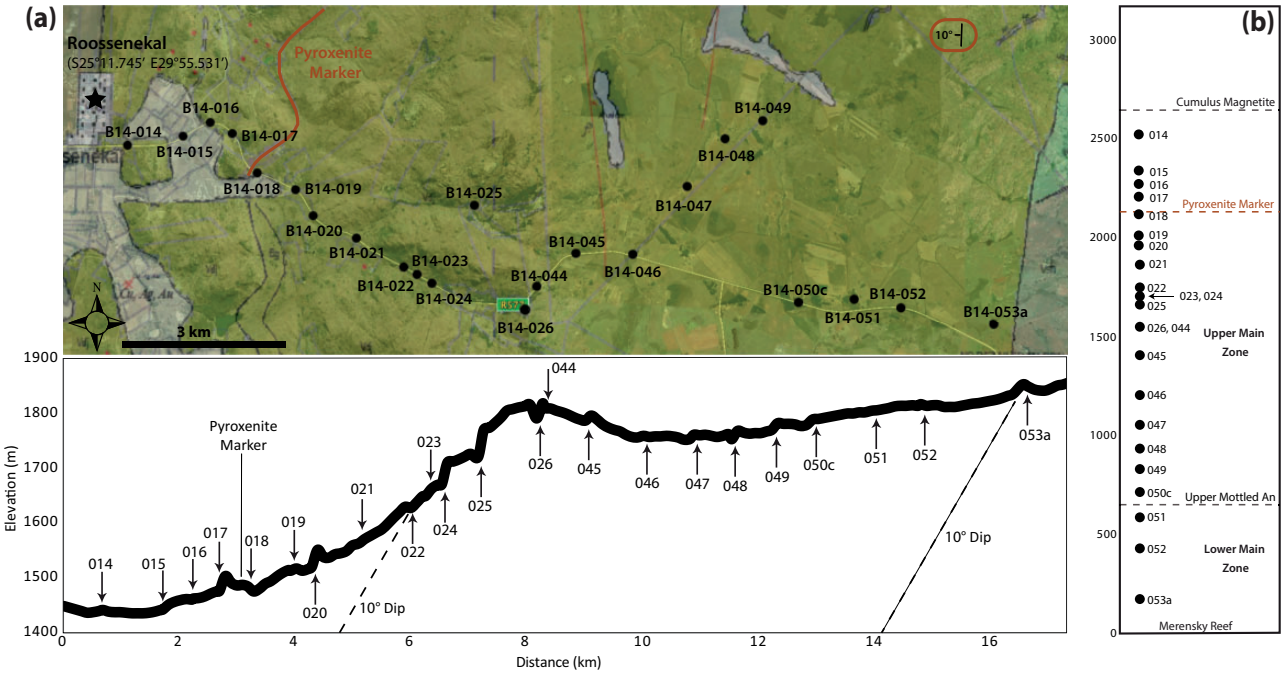

Fig. 3. (a) Snapshot of sample locations (black filled circles) for the Roossenekal Traverse overlain with the adapted geological map of Molyneux (2008). Topography from Google Earth (Map Data: © 2018 Google, AfriGIS (Pty) Ltd.; Image: 2018 DigitalGlobe). Below, elevation profile of the Roossenekal Traverse, perpendicular to strike, with the sample locations and other markers noted. The slightly different scale in the Google Earth image should be noted. Vertical exaggeration is 10. Horizontal distance 0 is the mapped Upper Zone–Main Zone boundary based on the appearance of cumulus magnetite. Image and elevation from Google Earth. (b) Constructed stratigraphic column for the Main Zone within the Eastern Limb at Roossenekal using a dip angle of 10°.

(measured via X-ray diffraction) and found that the maximum plagioclase An content in their three profiles decreased towards the south from An_{73} (~5 km south of Roossenekal) to An_{65} and An_{63}. They concluded that lateral variations in bulk plagioclase and orthopyroxene compositions were due to decreasing proportions of incoming magma as well as a change in the oxygen fugacity within the magma chamber; however, there was no attempt at quantifying the proportions or compositions of the magmas involved.

The most laterally extensive investigation into variability at the level of the Pyroxenite Marker of the Eastern Limb of the RLS to date was undertaken by Cawthorn *et al.* (2016). Cawthorn *et al.* (2016) compiled published data on plagioclase anorthite contents from eight profiles throughout the Eastern Limb, covering a lateral distance of 110 km. They showed that the maximum average plagioclase An content near the Pyroxenite Marker varies by only ~2 mol % (~An_{75} to An_{73}) from the Leolo Mountain Traverse of VanTongeren & Mathez (2013) to the first traverse just south of Roossenekal of Klemm *et al.* (1985)—a lateral distance of ~80 km. However, another 35 km to the south, at Stoffberg, the maximum An content of plagioclase is ~63 (Cawthorn *et al.*, 2016), yielding a decrease of maximum average plagioclase An content of ~12 An mol % over the ~110 km from the Leolo Mountain Traverse to Stoffberg. Cawthorn *et al.* (2016) concluded that changes in the stratigraphic level and the maximum plagioclase An content near the Pyroxenite Marker were controlled by a structural upwarp in the magma chamber basin. As is described in detail below (see Discussion section), there is no robust field evidence of a structural upwarp in this region. Thus, a different mechanism must be responsible for the lateral variability observed in maximum An content in the Eastern Limb by Cawthorn *et al.* (2016).

Lundgaard *et al.* (2006), although not focused on the recharge interval at the level of the Pyroxenite Marker, also investigated lateral variations within the mid to lower Main Zone of the Eastern Limb. The location of the three investigated profiles ranges from Thornhill in the north (analogous to the Leolo Mountain Traverse of this study) to Roossenekal and further south to Stoffberg (Fig. 1). They show that the average An content of plagioclase cores in the mid to lower Main Zone shows no systematic variation from north at Thornhill to south at Stoffberg. Conversely, there is a decrease in the Mg# of orthopyroxene cores (from Mg# 67–61 to 59–50), as well as in bulk plagioclase An content (from An 67–61 to 59–55), from Thornhill to Stoffberg. This change is coupled with an increase in the whole-rock concentration of incompatible elements from north at Thornhill to south at Stoffberg. Lundgaard *et al.* (2006) suggested that these lateral variations are a product of an increased trapped melt fraction from 0–10% in the north at Thornhill to 30–45% in the south at Stoffberg (Fig. 1). The lateral variations from Thornhill to Roossenekal are less pronounced and indicate an only

Downloaded from https://academic.oup.com/petrology/advance-article-abstract/doi/10.1093/petrology/egy081/5073045 by Rutgers University Libraries/Technical Services user on 02 October 2018

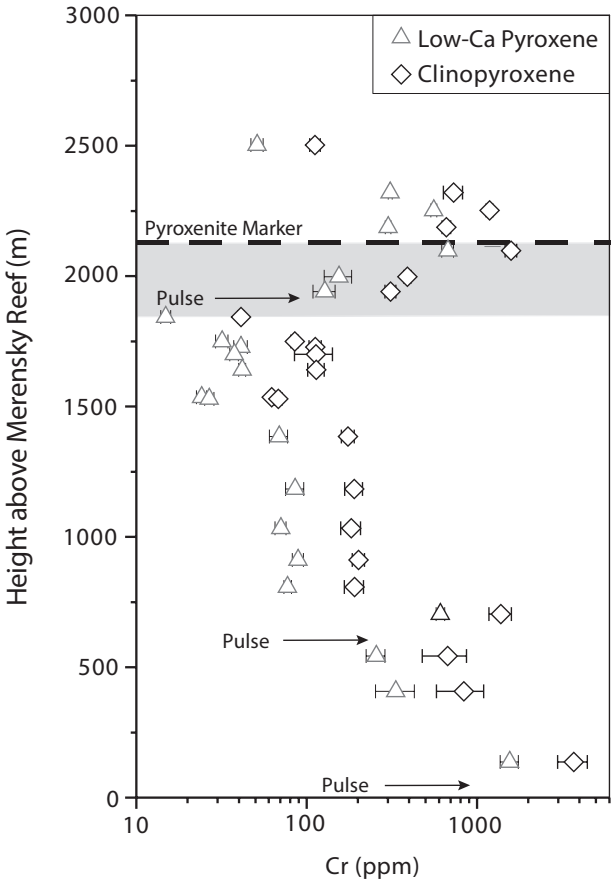

Fig. 4. Average Cr concentrations measured in cores of low-Ca pyroxene (open triangles) and clinopyroxene (open diamonds) throughout the entire Roossekenal traverse. Error bars denote 1σ standard deviation of the average Cr concentration for each sample. Dashed line denotes the level of the Pyroxenite Marker (PM). Shaded region is a graphic representation of the Zone of Magma Mixing from Table 3 and Fig. 2. Data from Table 2.

slight increase in trapped melt fraction at Roossenekal compared with Thornhill (Lundgaard *et al.*, 2006).

Apart from the study of Lundgaard *et al.* (2006), the conclusions deduced by the studies above rely primarily on the anorthite content of plagioclase. As noted above, these changes are sometimes extremely subtle and even within the uncertainties of average plagioclase anorthite content. Our study provides a comprehensive dataset of whole-rock and *in situ* mineral major element, as well as trace element compositions from a traverse of the Main Zone near Roossenekal (Figs 4–7). Our data from the Roossenekal Traverse, are compared with the data of VanTongeren & Mathez (2013) for the Leolo Mountain Traverse, ~75 km to the north. We calculate the proportion and composition of the incoming magma for both profiles using the method of VanTongeren & Mathez (2013). Our results provide a more robust quantification of the lateral variation in both the proportion of incoming versus resident magma and the composition of the incoming magma below the Pyroxenite Marker in the Eastern Limb of the RLS.

ANALYTICAL METHODS

Twenty-three samples of the Main Zone in the eastern RLS were collected along an approximately east–west traverse from Roossenekal (25°12·098′S, 029°55·907′E) to Draaikaal (25°13·849′S, 030°05·374′E) (Figs 1 and 3). The lack of well-defined layering in the Main Zone makes it difficult to constrain the dip of the rocks along the transect. Each sample was placed in its stratigraphic position by incorporating the elevation at each locality and using a shallow 10° dip as recorded in the lower Main Zone ~5 km north of the transect (Molyneux, 1974, 2008). The total thickness of the Main Zone at Roossenekal, using this dip angle, is ~2635 m. This is significantly less than the 3940 m thickness cited at Roossenekal by von Gruenewaldt (1973), which was calculated using a steeper dip angle of ~15°. There is evidence for steeper dip angles to the south at Stoffberg (up to 25°; Groeneveld, 1970); however, the scarcely recorded dips in the Roossenekal Traverse area are shallow: 10° in the lower Main Zone (Molyneux, 1974), and 10–12° in the Upper Zone (Scoon & Mitchell, 2012). All stratigraphic depths reported in this study are relative to the Merensky Reef at 0 m. A full list of samples with their stratigraphic height above the Merensky Reef and geographical location is provided in Table 1. The Pyroxenite Marker occurs at ~2133 m above the Merensky Reef in the Roossenekal Traverse.

The samples in this study consist of gabbronorites with nearly adcumulate textures and a cumulate mineral assemblage of 50–70% plagioclase, 15–30% low-Ca pyroxene and 5–20% clinopyroxene. Low-Ca pyroxene within the Main Zone is represented by a combination of primary orthopyroxene and inverted pigeonite, with inverted pigeonite becoming the primary low-Ca pyroxene below the Pyroxenite Marker. Modal abundances were estimated optically by point counting (minimum of 300 points per thin section).

Major element compositions for plagioclase, clinopyroxene and low-Ca pyroxene were determined using the JEOL JXA 8200 electron microprobe at Rutgers University and the Cameca SX100 microprobe at the American Museum of Natural History. All analyses used an acceleration potential of 15 kV, beam current of 15 nA, count time of 30 s on peak and 15 s on background for each element, and a beam diameter of 5 μm and 1 μm for plagioclase and pyroxene, respectively. Standards were analyzed between every ~50 unknowns and consistently yielded results within 2σ of published values (Supplementary Data Table S5; supplementary data are available for downloading at http://www.petrology.oxfordjournals.org).

In situ trace element compositions of plagioclase, clinopyroxene, and low-Ca pyroxene were obtained at Rutgers University using the Thermo Scientific iCAP Qc inductively coupled plasma mass spectrometry (ICP-MS) system equipped with a Photon Machines 193 nm laser ablation system. Spot sizes of 65 μm and 40 μm were used for plagioclase and pyroxene, respectively.

Downloaded from https://academic.oup.com/petrology/advance-article-abstract/doi/10.1093/petrology/egy081/5073045 by Rutgers University Libraries/Technical Services user on 02 October 2018

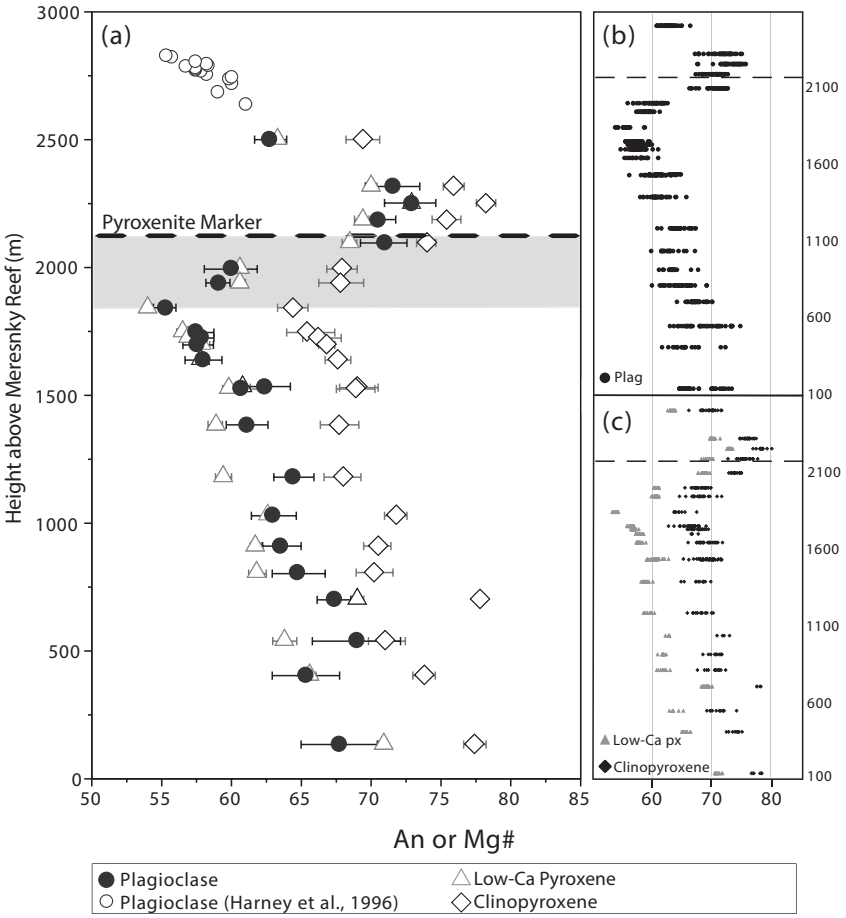

Fig. 5. (a) Average plagioclase An content (closed circles) and pyroxene Mg# (clinopyroxene, open diamonds; low-Ca pyroxene, open triangles) for the Roossenekal Traverse, plotted against stratigraphic height (m above the Merensky Reef). Error bars denote 1σ standard deviation of the average major element composition for each sample. Record of plagioclase An content is extended (open circles) using data from Harney *et al.* (1996). Dashed line denotes the level of the Pyroxenite Marker. Shaded region is a graphic representation of the Zone of Magma Mixing from Table 3 and Fig. 2. (b) Entire dataset of single plagioclase analyses. (c) Entire dataset of single low-Ca pyroxene and clinopyroxene analyses.

Approximately 10 s of gas backgrounds were collected before 30 s of sample ablation. Standards NIST610 and NIST612 were regularly analyzed for continuous calibration and to account for any drift. BCR and BIR were also analyzed regularly as a secondary standard to confirm accuracy (Supplementary Data Table S5).

In all samples collected for this study, thin section billets were cut perpendicular to the foliation and, where possible, parallel to the lineation so as to ensure that the thin section plane cuts through the center of alignment of the grains. Additionally, we were careful to only measure the center of cumulus grains and did not select grains with abnormal aspect ratios (possibly indicative of not being at the geometric center of the grain).

Major and trace element concentrations of bulk-rocks were determined using a ThermoARL Advant XP + sequential X-ray fluorescence (XRF) spectrometer at the Peter Hooper GeoAnalytical Lab at Washington State University. Replicate analyses of bulk-rocks were run from aliquots of the same crushed and powdered rocks.

Major and trace element compositions for plagioclase, clinopyroxene and low-Ca pyroxene are available in Supplementary Data Tables S1–S3. Whole-rock analyses for each sample are available in Supplementary Data Table S4.

RESULTS

Abrupt increases in Cr concentration are often interpreted as new fresh pulses of magma (e.g. Cawthorn, 2007; VanTongeren & Mathez, 2013; Tanner *et al.*, 2014). Three such increases occur within the Main Zone at Roossenekal. The first increase in Cr content occurs ~137 m above the Merensky Reef (Fig. 4). This study does not include any samples below this depth; however, the elevated Cr concentration in pyroxene is probably a consequence of the pulse(s) of magma responsible for forming the lower Main Zone. A distinctive second new pulse of magma is recorded in our section at ~704 m above the Merensky Reef (Fig. 4).

The third and final pulse of new magma into the RLS occurs ~270 m below the Pyroxenite Marker in

Downloaded from https://academic.oup.com/petrology/advance-article-abstract/doi/10.1093/petrology/egy081/5073045 by Rutgers University Libraries/Technical Services user on 02 October 2018

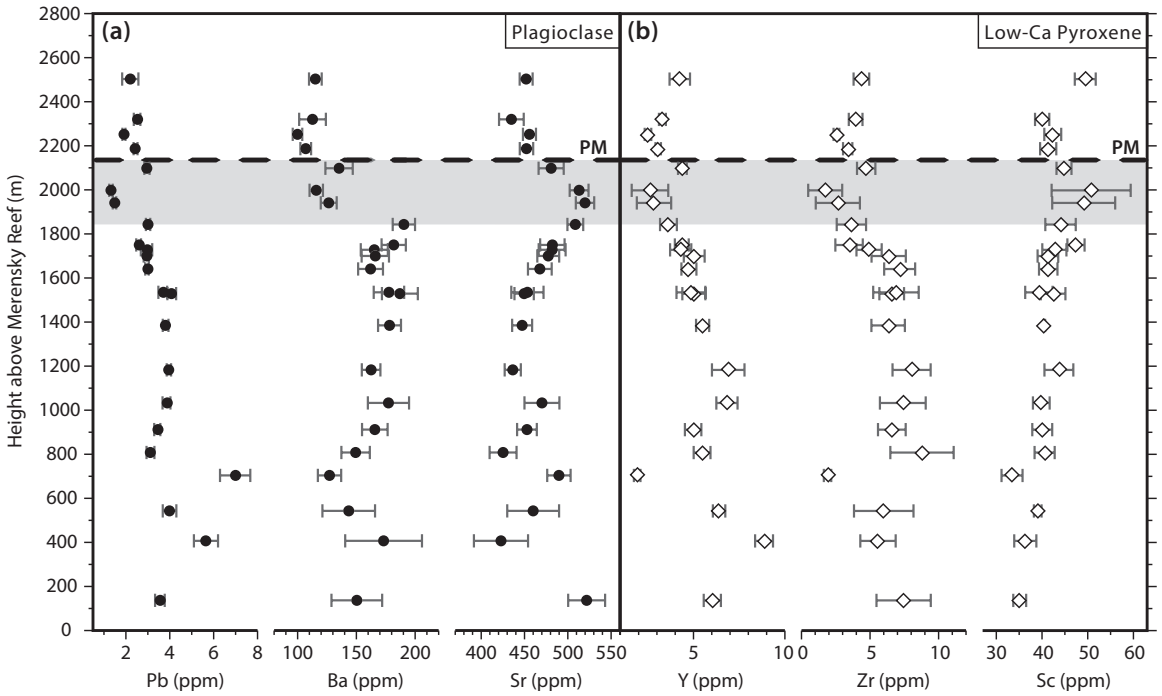

Fig. 6. Selected trace element concentrations, for which equilibrium liquid compositions are calculated, measured in cores of (a) plagioclase and (b) low-Ca pyroxene. Error bars denote 1σ standard deviation of the average trace element composition for each sample. Dashed line denotes the level of the Pyroxenite Marker (PM). Shaded region is a graphic representation of the Zone of Magma Mixing from Table 3 and Fig. 2. Data from Table 2. Varying scale on *x*-axis should be noted.

Roossenekal (Fig. 4). From ~704 m to 1750 m above the Merensky Reef, pyroxene Cr concentrations remain relatively low and constant upwards through the stratigraphy. At ~1750 m above the Merensky Reef, Cr concentrations begin to gradually increase over ~270 m until they reach a maximum just below the Pyroxenite Marker (Fig. 4). In contrast to the previous two pulses of new magma recorded by the Cr content, this interval of increasing Cr also coincides with reversals in the plagioclase An content (Fig. 5), pyroxene Mg# (Fig. 5), and whole-rock Sr isotopic compositions (Kruger *et al.*, 1987; Cawthorn *et al.*, 1991), as well as the formation of the Pyroxenite Marker. Therefore, it is likely that this final pulse of magma introduced a significantly larger volume of new magma into the resident Main Zone magma chamber.

Average plagioclase An contents and pyroxene Mg#s throughout the Main Zone of the Roossenekal Traverse are shown in Fig. 5a. Variations in measured plagioclase An content are similar to those reported by Cawthorn *et al.* (2016) at Roossenekal and those reported by VanTongeren & Mathez (2013) for the Leolo Mountain Traverse. The average An content of plagioclase decreases with increasing stratigraphic height within the lower Main Zone, reaching a minimum value of 55 at ~1843 m. Average plagioclase An values become progressively more primitive from ~1843 m above the Merensky Reef until they reach a maximum value of 73 at ~2252 m, ~119 m above the Pyroxenite Marker. Average low-Ca pyroxene and clinopyroxene Mg# follow the same trend as An content in plagioclase, with the maximum Mg# reaching 72·9 for low-Ca pyroxene and 78·2 for clinopyroxene. The reversal of An content in plagioclase and Mg# in pyroxene occurs at the same stratigraphic height with no evidence of decoupling as was described below the Pyroxenite Marker, within the Main Zone of the Western Limb (Nex *et al.*, 2002). The stratigraphic interval over which major element compositions of plagioclase and pyroxene become more primitive is hereafter termed the Zone of Magma Mixing, following VanTongeren & Mathez (2013). In the Roossenekal Traverse, studied here, the Zone of Magma Mixing occurs from 1843 m to 2133 m (Figs 2 and 5).

Figure 6 shows the stratigraphic variation of *in situ* trace element concentrations in plagioclase (Fig. 6a) and low-Ca pyroxene (Fig. 6b) from which equilibrium liquid compositions were calculated (Table 4). Although not as pronounced as those observed in major elements, incompatible trace elements measured *in situ* generally record decreases in concentration associated with the onset of magma mixing at ~1843 m above the Merensky Reef, whereas compatible trace elements generally increase (Fig. 6). REE concentrations in all mineral phases decrease within the Zone of Magma Mixing and are lowest in samples above the Pyroxenite Marker (Fig. 7).

Measured concentrations for trace elements to be used in magma mixing calculations are listed in Table 2 for plagioclase, low-Ca pyroxene and clinopyroxene, and full elemental data for each mineral can be found in the Supplementary Data.

Downloaded from https://academic.oup.com/petrology/advance-article-abstract/doi/10.1093/petrology/egy081/5073045 by Rutgers University Libraries/Technical Services user on 02 October 2018

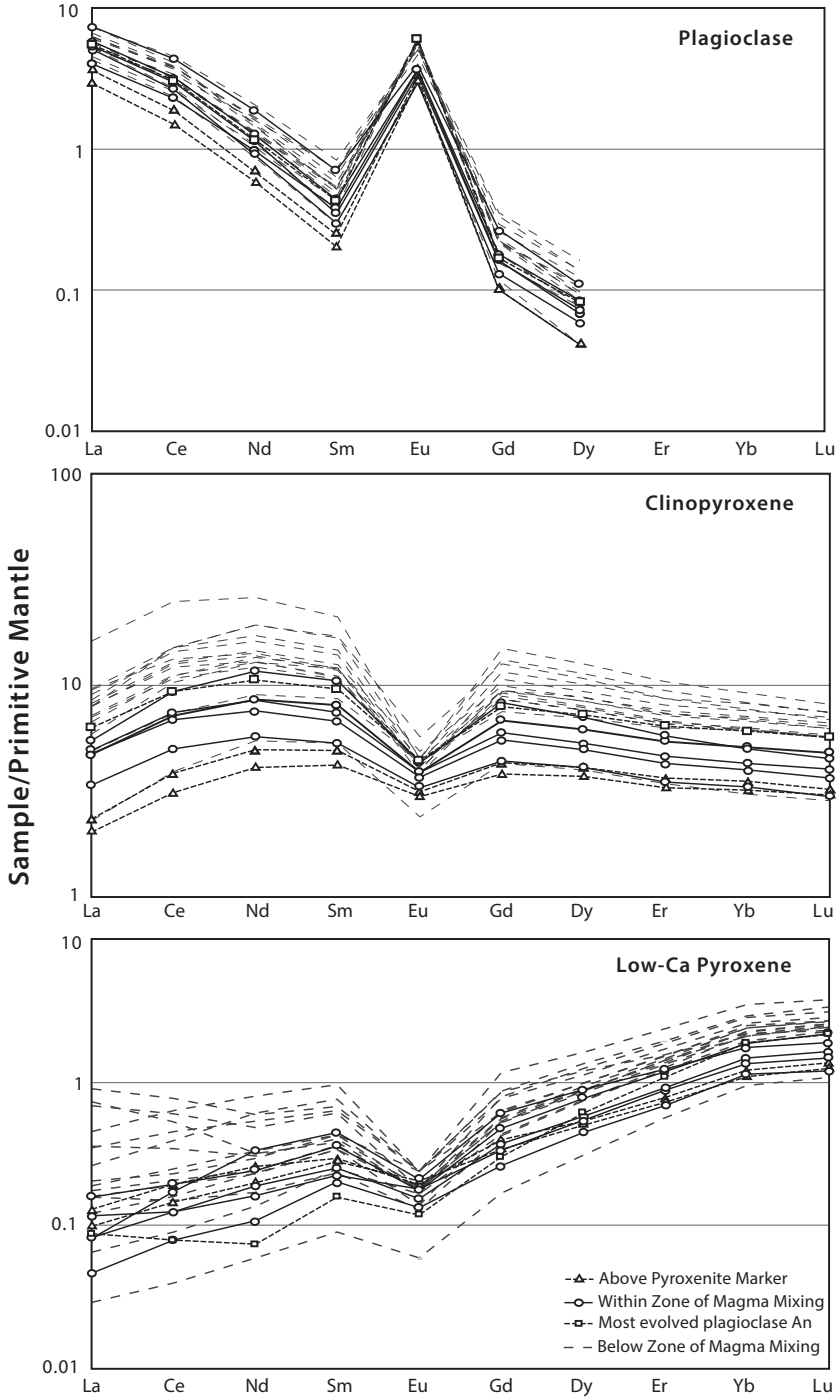

Fig. 7. REE compositions of each mineral phase for each sample throughout the Roossenekal Traverse. Data are normalized to the primitive mantle values of Sun & McDonough (1989). Dashed black line with open squares represents the most evolved sample below the Zone of Magma Mixing (B14-021). Continuous black line with open circles represents samples that are within the Zone of Magma Mixing. Dashed black line with open triangles represents samples above the Zone of Magma Mixing. All grey lines denote samples below the mixing interval. Data from Table 2.

Comparison of Leolo Mountain Traverse (north) and Roossenekal Traverse (south)

Mineral major element compositions

The level of the Pyroxenite Marker is similar in the two traverses, ~2200 m above the Merensky Reef in the north at Leolo and ~2133 m above the Merensky Reef in the south at Roossenekal. The maximum plagioclase An content, after the input of new primitive magma, is slightly higher in the north at Leolo than in the south at Roossenekal, with An contents of 76 and 73, respectively (Fig. 8a). Maximum pyroxene Mg#s also are slightly higher in the north at Leolo than in the south at Roossenekal, with the maximum Mg# of low-Ca pyroxene decreasing from 74 to 73 and clinopyroxene from

Downloaded from https://academic.oup.com/petrology/advance-article-abstract/doi/10.1093/petrology/egy081/5073045 by Rutgers University Libraries/Technical Services user on 02 October 2018

Table 1: Sample locations and stratigraphic depth (m above Merensky Reef)

Sample no.	Depth (m)	Latitude (S)	Longitude (E)
B14-053a	137	25°13·849′	30°05·374′
B14-052	407	25°13·692′	30°04·392′
B14-051	543	25°13·610′	30°03·892′
B14-050c	704	25°13·642′	30°03·294′
B14-049	808	25°11·863′	30°02·932′
B14-048	912	25°12·641′	30°02·521′
B14-047	1033	25°12·511′	30°02·104′
B14-046	1183	25°13·176′	30°01·509′
B14-045	1385	25°13·164′	30°00·893′
B14-044	1529	25°13·482′	30°00·471′
B14-026	1535	25°13·553′	30°00·397′
B14-025	1641	25°13·637′	29°59·707′
B14-024	1700	25°13·462′	29°59·328′
B14-023	1728	25°13·376′	29°59·165′
B14-022	1750	25°13·306′	29°59·016′
B14-021	1843	25°13·024′	29°58·485′
B14-020	1941	25°12·803′	29°57·999′
B14-019	1998	25°12·544′	29°57·800′
B14-018	2098	25°12·376′	29°57·366′
B14-017	2187	25°11·981′	29°57·082′
B14-016	2252	25°11·668′	29°56·828′
B14-015	2320	25°12·006′	29°56·524′
B14-014	2503	25°12·098′	29°55·907′

80 to 78 (Fig. 8b and c). The level at which the Zone of Magma Mixing begins (i.e. the most evolved plagioclase An content) is almost identical between the two profiles, with the most evolved sample at 1849 m above the Merensky Reef in the north at Leolo and 1843 m above the Merensky Reef in the south at Roossenekal. Overall, the major element variations (plagioclase An content and pyroxene Mg#) between the two traverses are small, pointing towards a remarkable consistency near the level of the Pyroxenite Marker over a distance of ~75 km.

Mineral major element differences between the Leolo and Roossenekal traverses are found primarily below the Zone of Magma Mixing. In the Leolo Traverse to the north, plagioclase An content is slightly higher prior to new magma input than in the south at Roossenekal. The most evolved low-Ca pyroxene Mg# prior to new magma input is ~65 at Leolo, whereas is ~54 at Roossenekal. Likewise, the clinopyroxene Mg# is 75 at Leolo, but 64 at Roossenekal prior to new magma input. Lundgaard *et al.* (2006) also found a similar offset in pyroxene Mg# between their Thornhill (northern) and Roossenekal traverses throughout the lower Main Zone.

Pyroxene Cr concentration

There is a significant decrease in the maximum Cr concentration of pyroxenes at the level of the Pyroxenite Marker from north to south. In the north, the Leolo Mountain Traverse records a maximum Cr concentration of 1630 ppm and 2480 ppm for low-Ca pyroxene and clinopyroxene, respectively (VanTongeren & Mathez, 2013). The maximum Cr concentration recorded at the same stratigraphic level in the south at Roossenekal is nearly half of that observed at Leolo, ~675 ppm for low-Ca pyroxene and 1590 ppm for clinopyroxene. Both traverses show pyroxene Cr concentrations within the Zone of Magma Mixing that are variable within a single sample.

Calculation of mixing parameters

Proportions

The proportion of incoming magma (X_{inc}) to resident magma (X_{res}) is inferred according the method outlined by VanTongeren & Mathez (2013), where the total magma thickness is equal to the sum of the resident magma thickness and the incoming magma thickness. The total thickness of the incoming magma is calculated as the stratigraphic excursion from the onset of magma mixing to the point at which the compositions return to their pre-mixing values (Figs 2 and 5). The thicknesses of each unit are based on average plagioclase core An content as it is more resistant to subsolidus re-equilibration than pyroxenes, owing to the coupled substitution of Ca–Al with Na–Si (Morse, 1984; Cherniak, 2003).

Calculation of total magma thicknesses at Roossenekal

Scoon & Mitchell (2012) collected a full stratigraphic record of the Upper Zone from multiple boreholes near Roossenekal and cited a total thickness of ~2300 m from the appearance of cumulus magnetite (Main Zone–Upper Zone boundary) to the roof of the intrusion. This thickness is significantly greater than the thickness for the same interval reported to the north near Magnet Heights (Fig. 2) of 1775 m (Molyneux, 1974). A detailed comparison of the UUMZ stratigraphy between the combined Leolo Mountain and Magnet Heights area (Molyneux, 1974) and the Roossenekal Traverse shows that individual magnetitite seams, as well as the first appearance of cumulus olivine, are traceable to remarkably similar stratigraphic levels over the ~75 km distance between the two traverses (Fig. 9). Stratigraphic thicknesses, however, deviate between the two profiles starting near the base of Subzone D (the appearance of cumulus apatite). It is at this point that the upper portion of the UUMZ becomes significantly thicker at Roossenekal than at Leolo. Within this portion of the stratigraphy, Magnetitite Seam 21 (the uppermost seam) also records varying thicknesses ranging from centimeter-scale near Magnet Heights (Molyneux, 1974) to >25 m thicknesses with some instances as much as 60 m recorded at Roossenekal (Scoon & Mitchell, 2012). We interpret this lateral continuity of marker layers within the Upper Zone as an indication that both traverses initially had roughly the same thickness during the UUMZ magma recharge event and any subsequent thickening in the uppermost portion of the Roossenekal Traverse is probably the result of a new magma pulse or assimilation affecting only the absolute last portions of the stratigraphy there.

Downloaded from https://academic.oup.com/petrology/advance-article-abstract/doi/10.1093/petrology/egy081/5073045 by Rutgers University Libraries/Technical Services user on 02 October 2018

Based on the geological map of Molyneux (2008), the stratigraphic interval from the Pyroxenite Marker to the appearance of cumulus magnetite (start of the Upper Zone) is ~521 m at Roossenekal and thus, assuming an original UZ thickness of 1775 m, as in the Leolo Mountain section of VanTongeren & Mathez (2013), the total magma thickness of the UUMZ from the Pyroxenite Marker to the roof at Roossenekal is 2296 m. Based on thermodynamic modelling and mineral–melt partition coefficients, VanTongeren *et al.* (2010) estimated that the UUMZ had lost ~15–25% of its original volume owing to eruption. Including this missing evolved melt, the total original UUMZ magma layer thickness is between 2640 and 2870 m.

In the traverse studied here, at Roossenekal, the Zone of Magma Mixing containing both resident and new incoming magma has a thickness of ~270 m and is calculated as the thickness from the onset of mixing (i.e. the depth of the most evolved plagioclase An content below the Pyroxenite Marker) to the Pyroxenite Marker (Figs 2 and 5). The total magma thickness, including the Zone of Magma Mixing and the UUMZ in Roossenekal, is calculated to be 2566 m (assuming 0% magma loss), and between 2910 and 3140 m (assuming 15–25% loss).

Calculation of total stratigraphic excursion

The total stratigraphic excursion caused by the new pulse of magma is calculated as the thickness from the onset of magma mixing below the Pyroxenite Marker to the level at which the An content in plagioclase returns to the composition prior to the onset of magma mixing [e.g. the most evolved sample below the Pyroxenite Marker (An 55)]. The samples from this study do not progress into the Upper Zone and consequently the An values of plagioclase in this study do not return to the most evolved value below the Pyroxenite Marker of An 55. An approximation of the thickness of the stratigraphic excursion can be obtained using the average plagioclase An compositions measured by Harney *et al.* (1996) from a single borehole, drilled ~2 km north of Roossenekal at Mapoch's Mine (Fig. 1) covering the lowermost ~200 m of the Upper Zone (above cumulus magnetite) in Roossenekal. Average plagioclase core An compositions return to pre-mixing compositions ~2824 m above the Merensky Reef (Figs 2 and 5). The total thickness from the Pyroxenite Marker until the return to pre-mixing compositions is 711 m, which when added to the Zone of Magma Mixing (270 m) yields a total excursion thickness of 981 m for the Roossenekal Traverse (Figs 2 and 5). This is less than the 1200 m thick excursion to the north in the Leolo Mountain Traverse calculated by VanTongeren & Mathez (2013).

All thicknesses cited above for the Roossenekal Traverse and the Leolo Mountain Traverse are summarized in Table 3. At Roossenekal, the proportion of incoming magma relative to the total is calculated to be 38, 34 and 31% for the scenarios of 0, 15 and 25% loss of original UUMZ magma thickness respectively (Table 3).

Resident, incoming, and mixed magma compositions

For a direct comparison of the resident and incoming magma compositions in the Zone of Magma Mixing from north to south, the equilibrium trace element liquid composition is calculated for each mineral phase of each sample. For ease of comparison, the equilibrium liquid compositions for the Roossenekal Traverse are calculated using the same partition coefficients as described by VanTongeren & Mathez (2013) for the Leolo Traverse. The Sr, Ba, Rb, Pb and light rare earth element (LREE) liquid compositions are calculated from plagioclase with the partition coefficients of Bindeman *et al.* (1998). REE liquid compositions are calculated from clinopyroxene with the partition coefficients of Wood & Blundy (1997); Sc, Y and heavy rare earth element (HREE) liquid compositions are calculated from orthopyroxene using the partition coefficients of Bédard (2007). D_{Zr}^{opx} and D_{Cr}^{opx} regressions with measured orthopyroxene Mg# do not show strong correlations (Bédard, 2007). Therefore, following VanTongeren & Mathez (2013), we use the constant $D_{Cr}^{opx} = 11{\cdot}5$ of Barnes (1986) derived for magmas at the quartz–fayalite–magnetite buffer (QFM) and 1150°C and the constant $D_{Zr}^{opx} = 0{\cdot}021$ of Dunn & Sen (1994) calculated for similar orthopyroxene major element compositions. When necessary, a pressure of 200 MPa is assumed. Following VanTongeren & Mathez (2013), the plagioclase and low-Ca pyroxene equilibrium liquid composition is used whenever possible, as they are a more reliable indicator of the equilibrium liquid owing to their higher modal abundance in the samples studied here.

Average crystallization temperatures are calculated for each sample using the REE-in-plagioclase–clinopyroxene thermometer developed by Sun & Liang (2017). The REE-in-plagioclase–clinopyroxene thermometer estimates the crystallization temperature of coexisting plagioclase and clinopyroxene. Through numerical simulations, Sun & Liang (2017) showed that the calculated crystallization temperatures are resistant to any artifacts from compositional zoning and diffusive resetting. The REE thermometer is potentially a significant improvement to An-based thermometers owing to the variability in An content of plagioclase (Fig. 5b) as well as the large uncertainties of plagioclase crystallization temperatures in previous low-pressure experiments (e.g. Charlier & Grove, 2012). Although it is an improved method for estimating crystallization temperatures, it should also be noted that calculated crystallization temperatures for the Leolo Mountain Traverse of VanTongeren & Mathez (2013) using the REE thermometer are in close agreement with the An-based thermometer used by VanTongeren & Mathez (see fig. 8b of Sun & Liang, 2017). The calculated equilibrium liquid and crystallization temperature for each sample is listed in Table 4.

Maximum crystallization temperatures near the level of the Pyroxenite Marker decrease from 1181°C for the

Downloaded from https://academic.oup.com/petrology/advance-article-abstract/doi/10.1093/petrology/egy081/5073045 by Rutgers University Libraries/Technical Services user on 02 October 2018

Leolo Mountain Traverse to 1166°C for the Roossenekal Traverse. Prior to the Zone of Magma Mixing, the crystallization temperature of the most evolved sample below the Pyroxenite Marker (analogous to resident magma) decreases from 1105°C for the Leolo Mountain Traverse to 1075°C (Fig. 10).

The composition of the fully mixed magma (C_{UUMZ}) at Roossenekal is calculated from the average trace element equilibrium liquid composition of samples B14-018 and B14-016. Sample B14-018 (~35 m below the Pyroxenite Marker) records the highest calculated crystallization temperature (1166°C) above the onset of magma mixing as well as the highest Cr concentration in both low-Ca pyroxene and clinopyroxene. Although sample B14-016 is located ~119 m above the Pyroxenite Marker, it also records a similarly high crystallization temperature of 1162°C as well as elevated Cr concentrations in low-Ca pyroxene and clinopyroxene. More importantly, sample B14-016 records the maximum plagioclase An content. The calculated composition of the fully mixed magma (C_{UUMZ}) at Roossenekal (Table 5) is similar to that calculated for the Leolo Mountain Traverse of VanTongeren & Mathez (2013) (Table 5).

The composition of the resident magma (C_{res}) is calculated from the most evolved sample (B14-021) below the onset of magma mixing, 270 m below the Pyroxenite Marker. The calculated resident magma compositions, prior to the Zone of Magma Mixing, are shown in Fig. 11a. Compositions of moderately incompatible trace elements, Sc and Sr, are indistinguishable between the calculated resident magma compositions at Leolo and Roossenekal. Highly incompatible trace elements [Ba, Zr, LREE, middle REE (MREE)], however, are higher in the south and indicate a slightly more evolved resident magma in the south. Notably, there are a few exceptions; the incompatible elements Y, Er, Yb and Lu all show slightly lower concentrations at Roossenekal. The only trace element with a compatible bulk partition coefficient, Cr, is slightly lower in the south.

The composition of the incoming magma below the Pyroxenite Marker is calculated following a two-component mixing equation (VanTongeren & Mathez, 2013)

$$C_{UUMZ} = C_{res}X_{res} + C_{inc}X_{inc} \quad (1)$$

where X_{res} and X_{inc} are the proportions of resident and incoming magma, and C_{UUMZ}, C_{res}, and C_{inc} are the fully mixed UUMZ parent magma composition, and the composition of the resident and incoming magmas.

For Roossenekal, the range of calculated incoming magma compositions, as well as the mineral phase from which each element was calculated, is given in Table 5 along with the range of incoming magma compositions for the Leolo Mountain Traverse (VanTongeren & Mathez, 2013), re-calculated using the REE-in-plagioclase–clinopyroxene thermometer described above (Sun & Liang, 2017). Rb is excluded in the calculations at Roossenekal because of high uncertainties in the measurement of low Rb concentrations.

The proportion of incoming magma calculated at Roossenekal is nearly identical to the proportion calculated ~75 km to the north by VanTongeren & Mathez (2013) (Table 3). For the 0% loss of original UUMZ magma thickness scenario, the proportion of incoming magma decreases from 43% in the north at Leolo (VanTongeren & Mathez, 2013) to 38% at Roossenekal (Table 3).

Focusing on the 0% UUMZ magma loss scenario for simplicity, the composition of the incoming magma is similar between the two profiles, although there is a slight enrichment in incompatible trace elements and depletion in compatible trace elements (e.g. Cr) from north to south (Table 5; Fig. 11b). The incoming magma calculated at Roossenekal also displays a prominent negative Eu (and Sr) anomaly, possibly indicating potential fractional crystallization of the incoming magma from north to south; however, there is no significant change in the modal abundance of plagioclase for a given stratigraphic level between the Leolo Mountain and Roossenekal traverses.

DISCUSSION

Lateral variations from trapped liquid?

Lundgaard *et al.* (2006) investigated the lateral variations within the mid to lower Main Zone (below the injection of new magma) in the Eastern Limb and attributed decreases in pyroxene Mg# and increases in whole-rock trace element compositions to be a product of increased trapped melt from north (near Thornhill; ~24°30·320′S, 030°59·194′E) to south (near Stoffberg; ~25°31·060′S, 029°54·752′E) (Fig. 1). Our data from the lower Main Zone near Roossenekal and the Leolo Mountain Traverse also support the conclusion that there was a greater fraction of trapped liquid present in the south compared with the north (Fig. 12a–e).

The trapped liquid shift, however, is not a factor in the lateral changes noted in this study over the Zone of Magma Mixing from Leolo to Roossenekal (Fig. 13a–e). Within the Zone of Magma Mixing, a plot of whole-rock Mg# versus whole-rock incompatible trace element concentrations (P, Ba, Zr, Rb) shows no noticeable shift from the Leolo Mountain to Roossenekal Traverse (Fig. 13b–e). Orthopyroxene Mg# and plagioclase An contents also appear to follow the same fractional crystallization trend between the Leolo Mountain and Roossenekal traverses over the Zone of Magma Mixing (Fig. 13a), but are offset from one another in the Lower Main Zone samples (Fig. 12a). Thus, we are confident that all lateral changes observed between the two traverses within the Zone of Magma Mixing are a true representation of a changing incoming magma composition.

Lateral variability owing to structural upwarp?: the Cawthorn *et al.* (2016) model

Cawthorn *et al.* (2016) suggested that the vertical and lateral variations in plagioclase An content are controlled by the injection of new magma into a structural

Downloaded from https://academic.oup.com/petrology/advance-article-abstract/doi/10.1093/petrology/egy081/5073045 by Rutgers University Libraries/Technical Services user on 02 October 2018

Table 2: Measured selected trace element compositions (ppm) in plagioclase, clinopyroxene and low-Ca pyroxene

Sample:	B14-014	B14-015	B14-016	B14-017	B14-018	B14-019	B14-020	B14-021	B14-022
Depth (m):	2503	2320	2252	2187	2098	1998	1941	1843	1750
Measured in plagioclase									
An content	62·70	71·52	72·86	70·45	70·93	59·95	59·04	55·24	57·42
Rb	0·67	1·00	0·83	0·46	0·58	2·48	2·47	1·58	1·32
Sr	451·88	434·84	455·72	452·27	480·76	513·04	519·86	508·67	482·17
Ba	115·09	112·67	99·90	106·61	138·96	115·85	126·46	190·41	181·76
Pb	2·20	2·51	1·91	2·44	2·96	1·32	1·48	3·01	2·58
La	2·76	4·01	3·53	3·72	5·09	2·02	2·48	3·79	3·61
Ce	4·06	5·74	4·67	5·29	7·74	2·65	3·32	5·40	4·79
Measured in clinopyroxene									
Mg#	69·4	75·9	78·2	75·4	74·0	67·9	67·8	64·4	65·4
La	3·22	3·37	2·30	3·24	3·75	1·38	1·60	4·32	3·33
Ce	12·72	13·23	8·83	12·16	16·55	5·50	6·80	16·59	13·02
Nd	11·55	11·49	7·72	10·22	15·80	5·52	6·69	14·35	12·18
Sm	3·56	3·29	2·35	2·99	4·67	1·85	2·18	4·25	3·84
Eu	0·65	0·65	0·55	0·62	0·72	0·50	0·53	0·74	0·74
Gd	4·06	3·54	2·60	3·29	4·92	2·27	2·56	4·73	4·45
Dy	4·54	3·90	3·01	3·66	5·22	2·73	3·02	5·35	5·17
Er	2·60	2·22	1·67	2·04	2·76	1·57	1·75	3·08	3·02
Yb	2·52	2·10	1·63	1·97	2·47	1·57	1·72	2·99	3·02
Lu	0·35	0·30	0·22	0·27	0·33	0·22	0·24	0·42	0·42
Measured in low-Ca pyroxene									
Mg#	56·9	57·9	57·8	60·8	59·8	58·9	59·4	62·6	61·7
Sc	49·46	40·03	42·35	41·35	45·44	50·75	49·12	44·05	47·43
Cr	51·31	310·14	557·83	300·91	675·42	155·17	127·73	14·91	31·87
Y	4·25	3·30	2·51	3·07	4·63	2·62	2·84	3·63	4·36
Zr	4·37	3·95	2·55	3·37	4·93	1·73	2·65	3·64	3·47
Gd	0·28	0·22	0·16	0·20	0·36	0·20	0·24	0·18	0·26
Dy	0·57	0·43	0·33	0·40	0·65	0·37	0·39	0·45	0·56
Er	0·57	0·44	0·33	0·42	0·59	0·35	0·37	0·52	0·61
Yb	0·92	0·73	0·56	0·67	0·86	0·54	0·60	0·93	1·07
Lu	0·16	0·12	0·09	0·11	0·14	0·09	0·10	0·16	0·19
Sample:	B14-023	B14-024	B14-025	B14-026	B14-044	B14-045	B14-046	B14-047	B14-048
Depth (m):	1728	1700	1641	1535	1529	1385	1183	1033	912
Measured in plagioclase									
An content	57·79	57·49	57·92	62·34	60·64	61·07	64·36	62·91	63·47
Rb	1·52	1·06	1·32	0·89	0·95	0·96	0·66	0·53	1·25
Sr	481·90	477·40	467·68	453·35	449·56	447·25	436·42	470·12	452·82
Ba	165·25	166·10	162·06	177·70	187·01	178·02	162·53	177·29	165·69
Pb	2·94	2·93	2·96	3·68	4·09	3·81	3·96	3·85	3·43
La	4·04	3·88	3·11	5·11	4·50	4·35	3·62	4·28	3·59
Ce	5·74	5·72	4·58	7·21	6·48	6·51	4·49	6·76	5·63
Measured in clinopyroxene									
Mg#	66·2	66·8	67·6	69·0	68·9	67·7	68·0	71·8	70·5
La	4·84	4·04	5·44	5·48	6·53	5·64	6·61	5·84	4·91
Ce	19·17	18·26	22·34	21·67	23·69	22·85	26·80	26·78	19·81
Nd	16·44	17·41	18·64	17·52	19·08	19·64	23·35	26·10	17·40
Sm	4·74	5·34	5·20	4·84	5·32	5·54	6·51	7·46	4·92
Eu	0·71	0·69	0·72	0·72	0·75	0·82	0·72	0·76	0·68
Gd	5·10	5·63	5·47	5·10	5·60	5·91	6·89	7·83	5·27
Dy	5·64	6·48	5·90	5·62	6·22	6·41	7·45	8·39	5·76
Er	3·14	3·54	3·27	3·16	3·50	3·64	4·15	4·54	3·22
Yb	3·05	3·39	3·04	3·02	3·43	3·52	4·04	4·08	3·11
Lu	0·42	0·46	0·42	0·42	0·47	0·49	0·55	0·55	0·43
Measured in low-Ca pyroxene									
Mg#	56·9	57·9	57·8	60·8	59·8	58·9	59·4	62·6	61·7
Sc	42·70	41·29	41·36	39·31	42·43	40·51	43·69	39·84	40·05
Cr	41·08	37·59	41·85	24·19	26·86	68·95	85·54	70·69	89·01
Y	4·30	5·04	4·75	4·86	5·02	5·50	6·90	6·83	4·98
Zr	4·93	6·36	7·16	6·89	6·58	6·32	8·03	7·39	6·59
Gd	0·25	0·32	0·31	0·31	0·34	0·37	0·52	0·47	0·33
Dy	0·55	0·65	0·62	0·64	0·69	0·73	0·99	0·92	0·66
Er	0·59	0·68	0·64	0·68	0·70	0·74	0·93	0·90	0·66
Yb	0·96	1·11	1·03	1·04	1·18	1·18	1·43	1·39	1·12
Lu	0·17	0·19	0·18	0·18	0·20	0·20	0·25	0·23	0·19

(continued)

Downloaded from https://academic.oup.com/petrology/advance-article-abstract/doi/10.1093/petrology/egy081/5073045 by Rutgers University Libraries/Technical Services user on 02 October 2018

Table 2: Continued

Sample:	B14-049	B14-050c	B14-051	B14-052	B14-053a
Depth (m):	808	704	543	407	137
Measured in plagioclase					
An content	64·69	67·34	68·94	65·29	67·69
Rb	0·69	3·12	0·78	0·51	0·54
Sr	425·24	489·72	459·98	422·83	521·74
Ba	149·34	127·14	143·39	173·15	150·37
Pb	3·12	6·98	3·99	5·65	3·55
La	4·55	2·95	4·16	3·73	5·05
Ce	6·87	4·15	6·67	6·01	8·11
Measured in clinopyroxene					
Mg#	70·2	77·8	71·0	73·8	77·4
La	4·59	1·56	6·22	11·09	5·45
Ce	19·59	6·92	25·65	44·17	26·79
Nd	18·27	7·42	21·91	35·28	26·09
Sm	5·35	2·36	6·15	9·32	7·57
Eu	0·64	0·40	0·66	0·75	0·96
Gd	5·56	2·54	6·34	8·93	7·50
Dy	6·17	2·93	6·87	9·29	7·90
Er	3·43	1·64	3·85	4·98	4·15
Yb	3·31	1·50	3·72	4·51	3·79
Lu	0·46	0·21	0·52	0·60	0·51
Measured in low-Ca pyroxene					
Mg#	61·8	69·0	63·8	65·6	70·9
Sc	52·99	33·44	39·06	36·34	35·12
Cr	77·40	611·55	256·16	334·07	1560·01
Y	5·47	1·92	6·40	8·86	6·03
Zr	8·79	1·90	6·00	5·58	7·45
Gd	0·38	0·10	0·46	0·70	0·51
Dy	0·73	0·23	0·83	1·19	0·88
Er	0·73	0·27	0·82	1·14	0·75
Yb	1·22	0·47	1·27	1·72	1·08
Lu	0·20	0·08	0·21	0·28	0·17

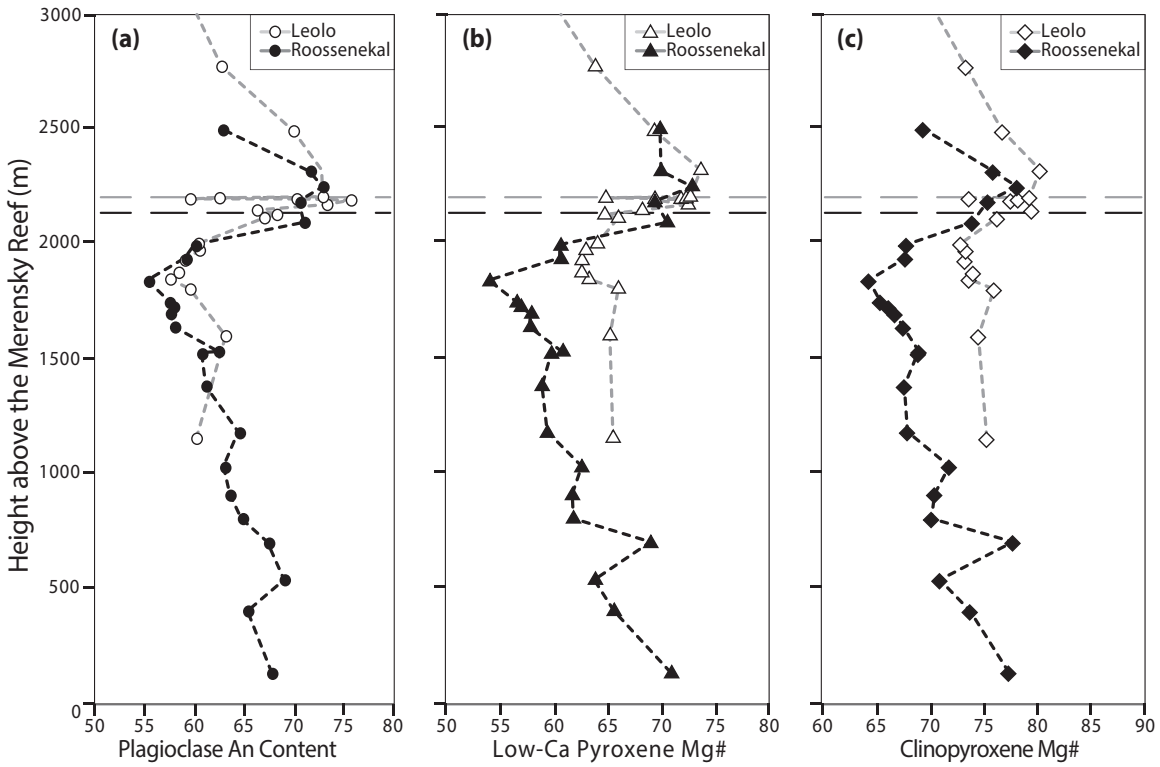

Fig. 8. Comparison of *in situ* major element compositions between the Roossenekal and Leolo traverses. The grey profile for each mineral phase represents the northern Leolo Traverse and the black profile represents the southern Roossenekal Traverse. The grey and black horizontal dashed lines represent the level of the Pyroxenite Marker for the Leolo and Roossenekal traverses, respectively. (a) Measured average An content of plagioclase cores. (b) Measured average Mg# of low-Ca pyroxene cores. (c) Measured average Mg# of clinopyroxene cores.

Downloaded from https://academic.oup.com/petrology/advance-article-abstract/doi/10.1093/petrology/egy081/5073045 by Rutgers University Libraries/Technical Services user on 02 October 2018

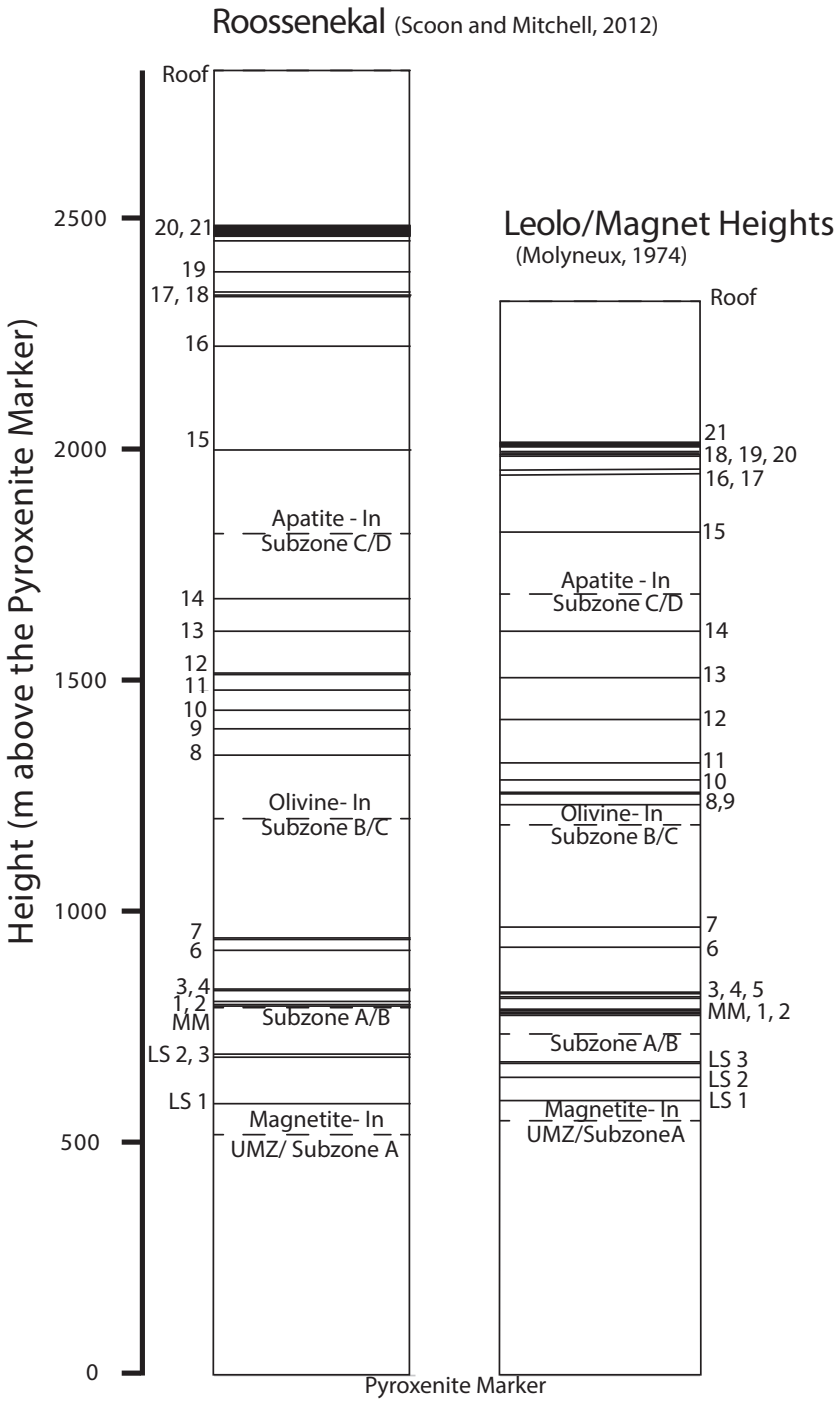

Fig. 9. Stratigraphic comparison of the UUMZ interval for both the combined Leolo–Magnet Heights and Roossenekal areas. *y*-axis is height (m) above the Pyroxenite Marker. Stratigraphic thicknesses for the Roossenekal Traverse in the Main Zone are from this study and in the Upper Zone from Scoon & Mitchell (2012). Stratigraphic thicknesses for the Leolo Mountain Traverse are from Molyneux (1974). Numerals to the side of each column denote magnetitite seams that are traceable throughout the Eastern Limb of the RLS.

basin. In their scenario, the new primitive magma is denser than the resident magma and is injected just south of Magnet Heights, into a structural basin that encompasses the northern portion of the Eastern Limb from the Leolo Mountains to some distance between Magnet Heights and Roossenekal, where the upwarp begins [see fig. 5 of Cawthorn *et al.* (2016)].

Evidence for a structural upwarp as described by Cawthorn *et al.* (2016) comes from map relationships just south of Roossenekal (Fig. 1) where the Critical Zone wedges out and the Main Zone is in contact with the floor rocks. In their model, the alleged structural upwarp would be controlled by floor rocks becoming ductile and developing into diapiric structures (e.g. Uken &

Downloaded from https://academic.oup.com/petrology/advance-article-abstract/doi/10.1093/petrology/egy081/5073045 by Rutgers University Libraries/Technical Services user on 02 October 2018

Table 3: Stratigraphic thicknesses and calculated proportions of incoming magma below the Pyroxenite Marker (PM) for both the Leolo and Roossenekal traverses

Transect	Leolo Mountain			Roossenekal		
% UUMZ magma loss:*	0	15	25	0	15	25
Zone of Magma Mixing (m)		350			270	
PM to return to pre-mixing An content (m)		850			711	
Total excursion thickness (m)		1200			981	
PM to roof (m)	2425	2850	3230	2296	2640	2870
Total magma thickness (m)	2775	3200	3580	2566	2910	3140
X_{inc} (%)	43	38	34	38	34	31

*UUMZ magma loss scenarios based on results of VanTongeren *et al.* (2010). Leolo Mountain values from VanTongeren & Mathez (2013).

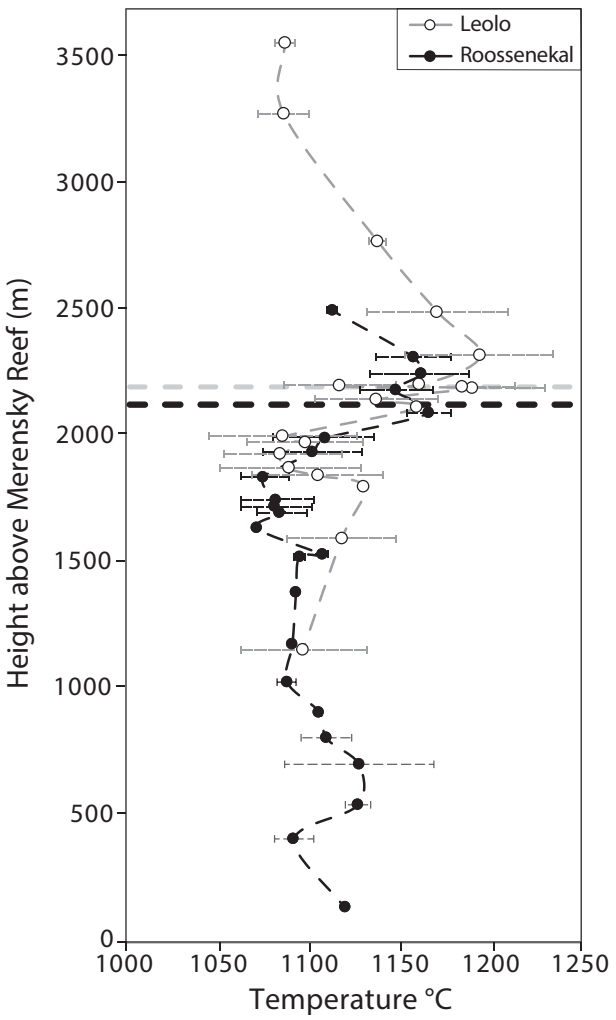

Fig. 10. Stratigraphic comparison of calculated crystallization temperatures for the Roossenkal (filled black circles) and Leolo (open grey circles) traverses plotted versus stratigraphic height (m above the Merensky Reef). Temperatures are estimates of the co-crystallization temperatures (or equilibrium temperatures) of plagioclase and clinopyroxene. (See text for full discussion.) Temperatures for the Leolo Traverse are from Sun & Liang (2017). Uncertainties are 1σ.

Watkeys, 1997). Although there is good evidence for basal diapirs and other structures affecting the lower parts of the intrusion elsewhere in the RLS, no such evidence exists in this area. An example is the pre-Bushveld Complex Schwerin anticlinal fold, located in the NE portion of the eastern Bushveld Complex. Schwerin fold deformation also occurred during the accumulation of the Lower Zone, forming separate magma compartments; however, its development was completed before the magma addition forming the Critical Zone (Cameron, 1978; Sharpe, 1982; Hartzer, 1995; Uken & Watkeys, 1997; Longridge *et al.*, 2009). It is clear from map relationships that the fold separates the lower portion of the Lower Zone into separate compartments, with the stratigraphy in the area dipping away from the axial center of the fold. Above this part of the stratigraphy in the region, all other markers and contacts are regionally parallel to those above, including the roof contact.

In contrast to the evidence in support of basal diapirs in the Lower Zone in the north, no such evidence exists for the Upper Zone–Main Zone in the area of Roossenekal. Field and map evidence in the southern portion of the Eastern Limb shows remarkably planar layering in the UUMZ cumulates that make up the top of the magma chamber. Detailed mapping by Molyneux (2008) shows that the layering in the UUMZ of the Eastern Limb of the RLS is regionally parallel to the roof contact. In particular, throughout the proposed areas of basinal upwarp of Cawthorn *et al.* (2016) (e.g. profiles just south of Roossenekal and the single profile near Stoffberg), the upper Magnetitite seam 21 is parallel to the roof contact. The Main Magnetitite seam is also mapped parallel to the roof contact through the area south of Roossenekal where Cawthorn *et al.* (2016) suggested the structural upwarp reaches its maximum. The Main Magnetitite seam is also mapped parallel to the roof contact when it reappears further south, near Stoffberg. The only observable exception is in a small area north and east of Loskop Dam, where Main Zone rocks directly abut the roof of the intrusion. These observations contradict the idea of having an upwarping basinal structure controlling the lateral variations within the UUMZ and Zone of Magma Mixing.

Instead, the presence of Main Zone rocks onlapping the floor of the intrusion near Stoffberg is more consistent with the gradual inflation and lateral expansion of the RLS magma chamber as a result of new volumetrically significant magma fluxes entering the crust

Downloaded from https://academic.oup.com/petrology/advance-article-abstract/doi/10.1093/petrology/egy081/5073045 by Rutgers University Libraries/Technical Services user on 02 October 2018

Table 4: Calculated crystallization temperature and equilibrium liquid composition (ppm) for each sample as calculated per listed mineral phase

Sample:	B14-014	B14-015	B14-016	B14-017	B14-018	B14-019	B14-020	B14-021	B14-022
Depth (m):	2503	2320	2252	2187	2098	1998	1941	1843	1750
T(°C):	1114	1158	1162	1148	1166	1109	1102	1075	1082
1σ:	4	25	33	27	17	30	31	14	23
Calculated from plagioclase									
Rb	21·75	39·39	33·84	17·84	21·94	74·36	72·99	46·46	38·72
Sr	199·34	246·42	267·65	248·35	269·24	209·81	206·58	190·73	180·92
Ba	436·89	617·11	579·29	563·82	733·79	387·40	407·26	576·93	550·26
Pb	6·58	11·36	9·22	10·55	12·89	3·43	3·68	6·96	5·97
La	14·56	18·82	19·28	20·22	27·21	10·44	12·81	19·78	18·80
Ce	30·81	35·15	38·41	42·88	61·56	19·42	24·24	39·66	35·10
Calculated from clinopyroxene									
La	36·15	38·41	25·10	36·14	47·68	15·61	17·87	44·79	35·85
Ce	93·65	100·61	64·50	89·98	140·08	40·74	49·52	111·15	90·65
Nd	44·16	46·80	30·34	40·24	71·07	21·23	25·08	48·93	43·18
Sm	9·35	9·39	6·49	8·21	14·59	4·90	5·59	9·85	9·24
Eu	1·54	1·68	1·38	1·53	2·03	1·19	1·21	1·54	1·60
Gd	8·92	8·53	6·09	7·60	12·91	5·02	5·45	9·12	8·90
Dy	9·48	9·00	6·76	8·09	12·98	5·74	6·10	9·80	9·80
Er	5·75	5·43	3·99	4·78	7·22	3·52	3·74	6·00	6·07
Yb	6·26	5·78	4·37	5·18	7·23	3·95	4·15	6·58	6·84
Lu	0·94	0·87	0·63	0·76	1·04	0·60	0·61	0·99	1·02
Calculated from low-Ca pyroxene									
Sc	41·57	33·66	36·15	34·66	37·95	40·64	39·33	34·08	37·18
Cr	4·46	26·97	48·51	26·17	58·73	13·49	11·11	1·30	2·77
Y	21·42	16·75	15·47	14·96	21·52	7·06	7·67	6·29	8·94
Zr	207·99	187·95	121·43	160·48	234·83	82·52	126·40	173·33	165·20
Gd	3·44	2·75	2·90	2·28	3·76	0·71	0·83	0·26	0·53
Dy	2·91	2·21	2·50	1·91	2·84	0·55	0·59	0·28	0·48
Er	2·50	1·95	1·83	1·79	2·39	0·76	0·82	0·69	0·98
Yb	2·80	2·24	2·19	1·96	2·39	0·77	0·85	0·77	1·08
Lu	0·35	0·27	0·25	0·23	0·27	0·09	0·10	0·09	0·13

Sample:	B14-023	B14-024	B14-025	B14-026	B14-044	B14-045	B14-046	B14-047	B14-048
Depth (m):	1728	1700	1641	1535	1529	1385	1183	1033	912
T(°C):	1081	1084	1071	1108	1095	1093	1091	1088	1106
1σ:	20	15	2	3	4	3	1	5	1
Calculated from plagioclase									
Rb	45·32	30·89	40·44	28·96	30·26	31·32	24·09	18·59	42·69
Sr	182·51	179·74	176·47	197·39	185·57	186·51	198·52	205·32	202·90
Ba	509·82	503·76	507·43	666·89	654·60	638·05	683·91	697·45	657·70
Pb	6·94	6·78	7·07	10·84	11·13	10·62	13·18	11·89	10·75
La	21·14	20·21	16·49	27·05	23·80	23·18	19·93	23·34	19·25
Ce	42·41	41·86	34·39	54·92	48·99	49·72	44·21	53·49	43·73
Calculated from clinopyroxene									
La	49·20	41·57	50·52	59·95	66·46	59·66	68·09	53·92	51·30
Ce	126·33	122·19	134·63	155·31	157·55	157·32	179·60	160·84	135·25
Nd	55·71	59·85	57·64	65·18	65·83	69·58	80·48	80·66	61·50
Sm	11·02	12·55	11·01	12·39	12·64	13·42	15·34	15·78	1·93
Eu	1·48	1·47	1·37	1·66	1·62	1·78	1·52	1·44	1·48
Gd	9·91	11·08	9·71	10·92	11·16	11·94	13·56	12·90	10·67
Dy	10·52	12·16	10·03	11·47	11·85	12·32	13·95	14·14	11·10
Er	6·27	7·07	5·95	6·84	7·11	7·42	8·26	8·14	6·58
Yb	6·94	7·66	6·28	7·37	7·90	8·09	9·08	8·27	7·16
Lu	1·03	1·11	0·94	1·09	1·17	1·21	1·32	1·20	1·06
Calculated from low-Ca pyroxene									
Sc	33·54	32·60	32·64	31·51	33·84	32·15	34·77	32·24	32·26
Cr	3·57	3·27	3·64	2·10	2·34	6·00	7·44	6·15	7·74
Y	9·06	11·35	10·63	13·29	12·85	13·25	17·19	21·09	14·48
Zr	234·52	302·98	340·95	328·03	313·14	300·95	382·38	351·90	313·81
Gd	0·55	0·79	0·75	1·14	1·07	1·04	1·55	2·16	1·35
Dy	0·50	0·68	0·64	0·98	0·93	0·87	1·26	1·79	1·14
Er	0·97	1·21	1·13	1·52	1·44	1·42	1·86	2·29	1·57
Yb	1·01	1·26	1·16	1·50	1·57	1·45	1·84	2·32	1·74
Lu	0·12	0·15	0·14	0·18	0·18	0·17	0·22	0·27	0·21

(continued)

Downloaded from https://academic.oup.com/petrology/advance-article-abstract/doi/10.1093/petrology/egy081/5073045 by Rutgers University Libraries/Technical Services user on 02 October 2018

Table 4: Continued

Sample:	B14-049	B14-050c	B14-051	B14-052	B14-053a
Depth (m):	808	704	543	407	137
T(°C):	1110	1128	1127	1092	1120
1σ:	14	41	7	11	2
Calculated from plagioclase					
Rb	24·44	115·14	30·51	19·26	20·59
Sr	197·25	245·84	240·64	197·30	263·28
Ba	625·92	592·87	722·40	761·36	719·27
Pb	10·38	26·27	16·33	19·74	13·71
La	24·58	15·97	22·88	20·70	27·69
Ce	54·08	33·08	54·59	49·03	65·78
Calculated from clinopyroxene					
La	49·17	14·51	69·21	99·24	44·73
Ce	137·38	42·79	188·42	257·70	144·56
Nd	66·53	24·41	84·73	106·32	73·59
Sm	13·39	5·44	16·49	19·27	14·73
Eu	1·44	0·84	1·60	1·40	1·68
Gd	11·64	4·95	14·30	15·46	12·23
Dy	12·30	5·51	14·80	15·35	12·29
Er	7·25	3·30	8·81	8·77	6·85
Yb	7·88	3·41	1·86	8·98	7·05
Lu	1·17	0·52	1·43	1·28	1·01
Calculated from low-Ca pyroxene					
Sc	32·69	27·97	31·80	29·87	29·67
Cr	6·73	53·18	22·27	29·05	135·65
Y	16·01	9·11	21·42	33·46	32·50
Zr	418·57	90·48	285·71	265·71	354·76
Gd	1·57	1·08	2·46	4·80	7·09
Dy	1·28	1·04	1·89	3·44	5·12
Er	1·75	1·12	2·29	3·64	3·58
Yb	1·91	1·33	2·34	3·68	3·58
Lu	0·22	0·16	0·27	0·42	0·40

associated with the Main Zone and Upper Zone. This alternative hypothesis is also consistent with the changing lithology of both roof and floor rocks from north to south in the Eastern Limb (e.g. VanTongeren & Mathez, 2015).

Another aspect of the Cawthorn *et al.* (2016) model is the requirement of a density stratified magma chamber. In their model, density differences constrain the incoming magma to the bottom of the chamber, while limiting the mixing between the incoming and resident magma. Limited mixing between the two magmas at the bottom of the chamber would inevitably lead to a rapid increase of crystallization temperature as well as a return to pre-mixing (more radiogenic) initial $^{87}Sr/^{86}Sr$ values of the original resident magma, above the Zone of Magma Mixing. However, recorded crystallization temperatures show a gradual increase up to the Pyroxenite Marker and fully mixed magma (i.e. cessation of input of new primitive magma; Fig. 10) while initial whole-rock $^{87}Sr/^{86}Sr$ values above the Pyroxenite Marker are relatively homogeneous, both arguing against a density stratified magma chamber.

A new hypothesis for magma recharge and lateral variability in the Eastern Limb

The data presented here (Fig. 11a and b) show that both the resident and incoming magmas in the Roossenekal Traverse are slightly more evolved than those observed in the north along the Leolo Mountain Traverse of VanTongeren & Mathez (2013). In their study, VanTongeren & Mathez (2013) suggested that the gradual compositional reversal throughout the Zone of Magma Mixing stratigraphy is due to repeated injection and mixing of small magma batches into a rapidly mixed homogeneous magma chamber. The repeated injection of small magma batches allowed the magmas to mix while continuing to crystallize. Our data from the Roossenekal Traverse support this hypothesis and allow us to additionally determine the directionality of magma emplacement.

We propose that new batches of primitive magma were periodically injected into the magma chamber near the Thabazimbi–Murchison Lineament (TML) as the magma chamber was inflated from north to south (Fig. 1). Our model is based on three observed differences between the Leolo Mountain Traverse in the north and the Roossenekal Traverse in the south: (1) the decrease in the calculated proportions of incoming versus resident magma from 43% in the north for the Leolo Mountain Traverse to 38% for the Roossenekal Traverse, ~75 km to the south (Table 3); (2) the slightly more evolved trace element composition of the resident magma towards the south at Roossenekal, accompanied by more evolved major element compositions towards the south below the Zone of Magma Mixing (Figs 8 and 11a); (3) the slightly more evolved trace element composition of the calculated incoming magma in the south relative to the north, as well as the shift to a more

Downloaded from https://academic.oup.com/petrology/advance-article-abstract/doi/10.1093/petrology/egy081/5073045 by Rutgers University Libraries/Technical Services user on 02 October 2018

Table 5: Calculated incoming magma composition (ppm) below the Pyroxenite Marker for the Leolo Mountain and Roossenekal traverses

	Leolo Mountain*					Roossenekal				
	C_{UUMZ}	C_{res}	C_{inc}			C_{UUMZ}	C_{res}	C_{inc}		
			0%	15%	25%			0%	15%	25%
Sc^{opx}	36	37	35	34	34	37	34	42	43	44
Cr^{opx}	108	5	245	283	317	54	1	139	155	170
Rb^{plag}	24	33	13	10	7	—	—	—	—	—
Sr^{plag}	245	176	335	361	384	268	191	395	419	441
Y^{opx}	21	11	34	38	41	19	6	38	42	46
Zr^{opx}	192	141	260	279	296	178	173	186	187	189
Ba^{plag}	468	334	644	695	738	657	577	786	811	834
La^{plag}	14·68	14·32	15·17	15·30	15·42	23·25	19·78	28·90	29·97	30·96
Ce^{plag}	32·19	30·93	33·87	34·35	34·77	49·99	39·66	66·83	70·03	72·97
Nd^{cpx}	27·97	24·81	32·17	33·37	34·40	50·71	48·93	53·60	54·15	54·66
Sm^{cpx}	6·13	5·43	7·06	7·32	7·55	10·54	9·85	11·67	11·88	12·08
Eu^{cpx}	1·31	0·96	1·77	1·90	2·02	1·71	1·54	1·97	2·03	2·07
$Gd^{cpx,opx}$	5·13	3·52	7·26	7·87	8·40	6·42	4·69	9·23	9·76	10·26
$Dy^{cpx,opx}$	4·87	3·88	6·19	6·56	6·88	6·27	5·04	8·28	8·66	9·01
Er^{opx}	1·96	1·12	3·07	3·39	3·67	2·11	0·69	4·43	4·87	5·28
Yb^{opx}	2·17	1·21	3·44	3·80	4·12	2·29	0·77	4·76	5·23	5·67
Lu^{opx}	0·29	0·18	0·44	0·48	0·51	0·26	0·09	0·54	0·60	0·65

*Values for the Leolo Mountain Traverse are recalculated from VanTongeren & Mathez (2013) utilizing the calculated plagioclase crystallization temperatures of Sun & Liang (2017).

evolved plagioclase An content from north to south within the Zone of Magma Mixing (Figs 8 and 11b).

In our model (Fig. 14), as in that of VanTongeren & Mathez (2013), pulses of new primitive magma mix with resident magma, up to the immediate roof, while simultaneously crystallizing between pulses. However, in our model, owing to the directed injection of new primitive magma from the TML, the proportion of incoming magma mixing with resident magma decreases slightly towards the south. Each new pulse of magma fully mixes with the resident magma in the north and gradually inflates the magma chamber by mixing over a progressively wider lateral area. During the initial recharge events, the proportion of new magma is small enough in volume that it remains dominantly in the north. However, as new pulses are added the amount of incoming magma increases and the mixed magma spreads into the resident magma in the south. The resident magma in the south thus has a longer period of time to undergo fractionation and hence the resident magma records slightly more evolved compositions prior to the onset of magma mixing in Roossenekal as compared with Leolo. In both Leolo and Roossenekal, fractional crystallization on the magma chamber floor probably proceeded *in situ* in a small (<4 m) thick mush layer (e.g. Holness *et al.*, 2017), such that mixing between the incoming magma and any previously formed crystals from the resident magma would occur only at a scale smaller than our sampling interval and would not be recorded in our dataset. Thus, the slightly more evolved compositions recorded in the resident magma at Roossenekal are a robust indicator of fractionation of the liquid prior to new magma input, and not simply a greater proportion of mixing with a resident magma.

Our directional recharge scenario is consistent with the muted and/or lack of reversal recorded in plagioclase An content much farther south, at Stoffberg (e.g. Cawthorn *et al.*, 2016; Fig. 1), as this is where the proportion of new incoming magma would be predicted to be the least. This scenario also explains why the incoming magma is slightly more evolved in the south. Incompatible trace element concentrations of the calculated incoming magma (C_{inc}) increase from north to south, whereas Cr concentrations decrease from 245 ppm to 181 ppm for the Leolo Mountain and Roossenekal traverses, respectively. C_{inc} for Roossenekal shows a slightly more negative Eu anomaly (Eu/Eu* = 0·56) than that recorded from the relatively flat REE profile of C_{inc} for the Leolo Mountain Traverse of VanTongeren & Mathez (2013) (Eu/Eu* = 0·76; Fig. 11b). Thus, if the incoming magma were of a homogeneous composition, it must have experienced some degree of fractional crystallization in the north, prior to entering and mixing with the resident magma in the south.

Numerous researchers have also postulated that the locus of magma injection in the Eastern Limb is near the TML (e.g. Kruger, 2005; Clarke *et al.*, 2009; VanTongeren & Mathez, 2015) (Fig. 1). On the basis of structural and compositional evidence, Clarke *et al.* (2009) concluded that a feeder dike used the existing TML to fill the RLS magma chamber, inflating the chamber away from the TML (i.e. to the north and south of the TML). Investigating the variability in the immediate roof and floor lithologies of the Bushveld Complex (Fig. 1), VanTongeren & Mathez (2015) presented a model in which the RLS was intruded as an enormous sill occupying varying structural depths (deeper in the

Downloaded from https://academic.oup.com/petrology/advance-article-abstract/doi/10.1093/petrology/egy081/5073045 by Rutgers University Libraries/Technical Services user on 02 October 2018

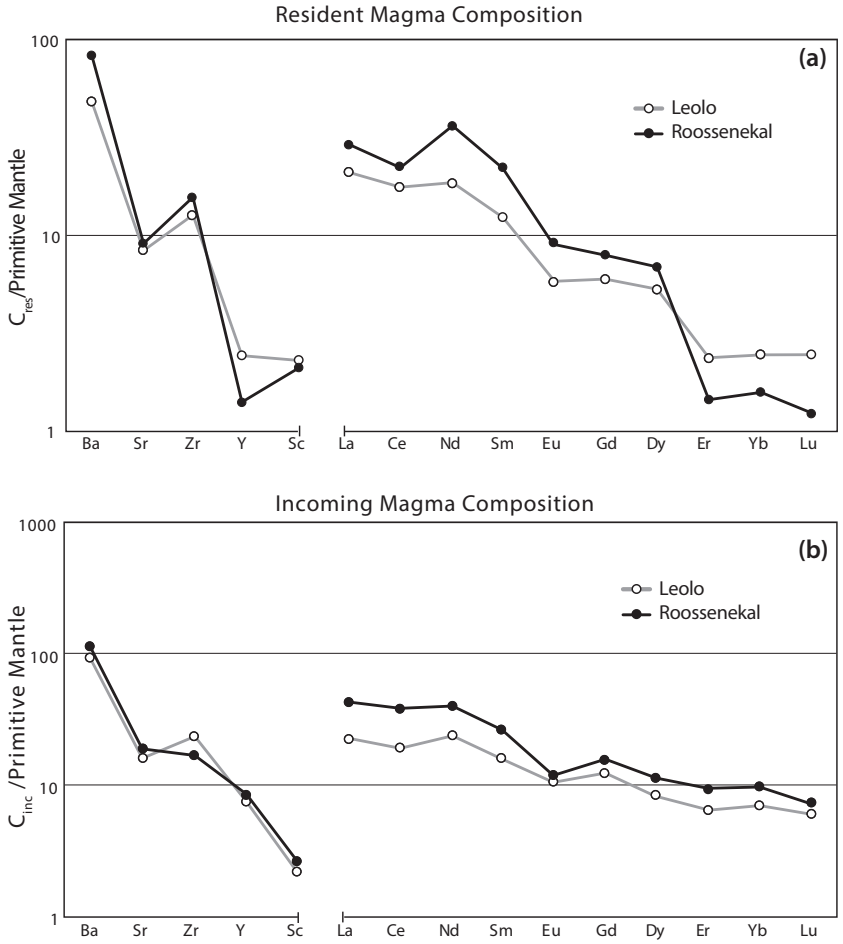

Fig. 11. Comparison of calculated resident and incoming magma compositions, assuming a 0% magma loss scenario, normalized to the primitive mantle values of Sun & McDonough (1989) between the Leolo and Roossenekal traverses. Primitive mantle values for Sc are from McDonough & Sun (1995). (a) Resident magma compositions. Leolo resident magma composition from VanTongeren & Mathez (2013). (b) Incoming magma compositions. Leolo incoming magma composition recalculated from VanTongeren & Mathez (2013) using the updated crystallization temperatures of Sun & Liang (2017). Data from Table 5.

north and shallower in the south), consistent with the locus of the magma injection originating in the north near the TML. Kruger (2005) similarly postulated that the Main Zone magmas were input into the magma chamber, just north of the TML, first interacting with the floor rocks to produce the Platreef, locking in higher initial $^{87}Sr/^{86}Sr$ ratios, before spreading south and mixing with the residual Critical Zone magma. In the model of Kruger (2005), incoming Main Zone magma spreads south and mixes with the residual Critical Zone magma, which has a lower initial $^{87}Sr/^{86}Sr$ ratio, to produce the average $^{87}Sr/^{86}Sr$ ratio in the Lower Main Zone of ~0·7086.

Reliability of the pyroxene record?

As a final note, it is important to consider the reliability of the cumulate record when calculating magma compositions and inferring magma dynamics. For example, in their study, VanTongeren & Mathez (2013) observed the rapid increase in Cr contents of pyroxenes within the Zone of Magma Mixing up to the Pyroxenite Marker, followed by a rapid return to their pre-mixing values. They also noted that the Pyroxenite Marker exhibits a lower whole-rock Sr isotopic composition than both the Main Zone and the UUMZ, and hypothesized that the pyroxenes within the Zone of Magma Mixing may have been intruded within the incoming magma as a crystal cargo. The pyroxene Cr contents within the Zone of Magma Mixing at Roossenekal, although overall lower, agree with the hypothesis of VanTongeren & Mathez (2013) that the pyroxenes were intruded as a crystal cargo.

At Roossenekal, both low-Ca pyroxene and clinopyroxene Cr contents show the same rapid increase to the Pyroxenite Marker and return to pre-mixing values (Fig. 4) as seen within the Leolo Mountain Traverse. The calculated equilibrium liquid composition for Cr just below the Pyroxenite Marker is ~59 ppm, whereas just 400 m above this value returns to ~4 ppm. Simple Rayleigh fractional crystallization modelling indicates that this change in Cr composition would require ~55% crystallization over the 400 m stratigraphic interval.

Downloaded from https://academic.oup.com/petrology/advance-article-abstract/doi/10.1093/petrology/egy081/5073045 by Rutgers University Libraries/Technical Services user on 02 October 2018

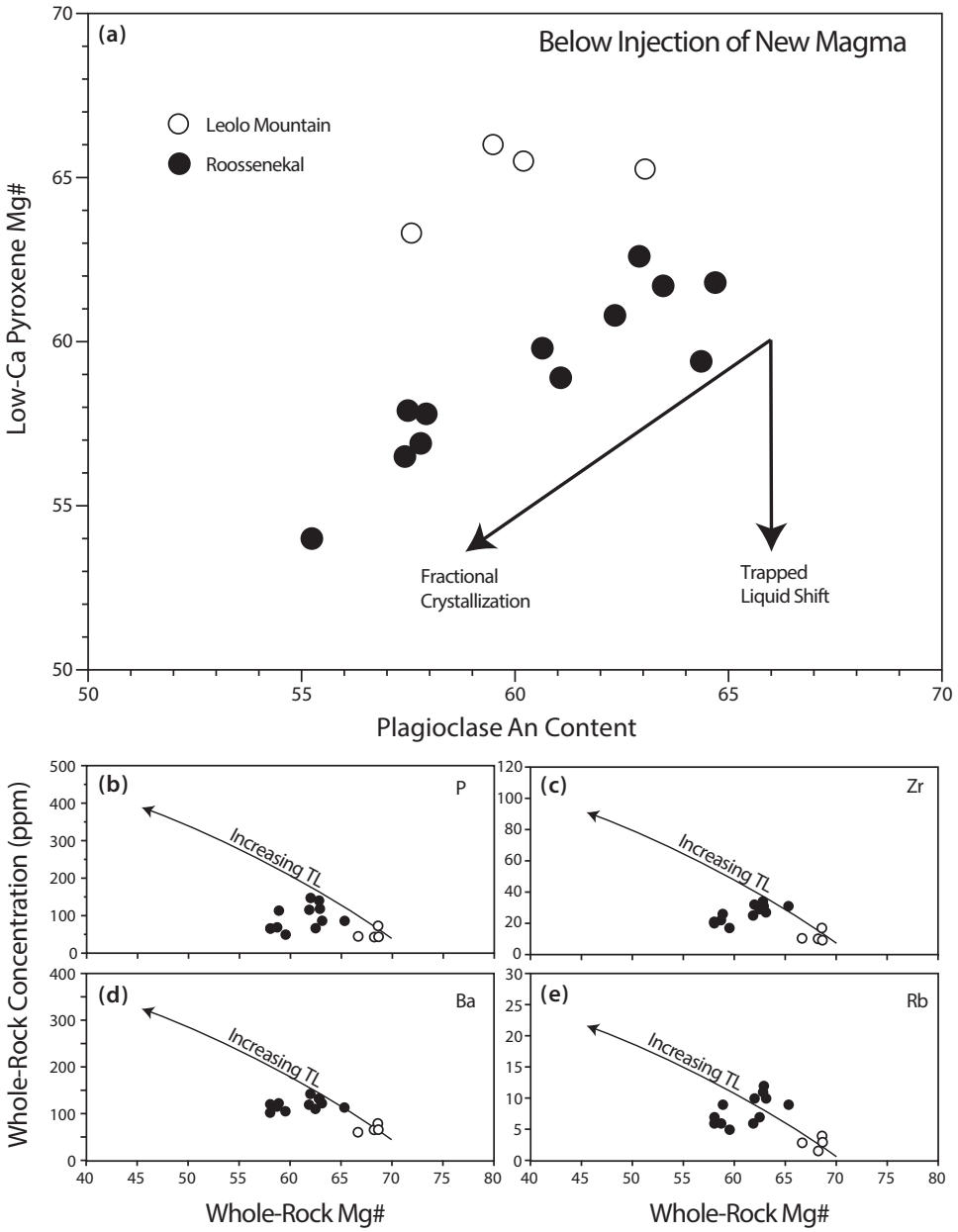

Fig. 12. (a) Average plagioclase core An content versus average low-Ca pyroxene core Mg#. (b–e) Whole-rock Mg# versus selected whole-rock incompatible trace element concentrations (P, Zr, Ba, Rb) for both the Leolo Mountain and Roossenekal traverses. Only samples from below the Zone of Magma Mixing are shown. The offset between the two traverses supports the conclusion of Lundgaard *et al.* (2006) of a slight increase in the trapped liquid fraction within the lower Main Zone from north (Leolo) to south (Roossenekal).

Assuming 0% magma loss from the UUMZ, this 400 m interval accounts for only ~17% of the UUMZ stratigraphy and therefore it is unlikely that fractional crystallization can account for reversal of pyroxene Cr compositions and their rapid return to pre-mixing values.

As mentioned above, below the Zone of Magma Mixing the Mg# of low-Ca pyroxene and clinopyroxene decreases considerably from north to south (Fig. 8). In the lower Main Zone, Lundgaard *et al.* (2006) attributed this decrease to an increased fraction of trapped liquid resetting the relatively fast-diffusing Fe–Mg cations. As shown above, however, this explanation does not apply to the cumulates within the Zone of Magma Mixing, where the two profiles reach similar Mg#s at similar stratigraphic intervals for both low-Ca pyroxene and clinopyroxene. Instead, an alternative explanation for the reversal in major element compositions of pyroxene within the Zone of Magma Mixing incorporates low-Ca pyroxene and clinopyroxene as a crystal cargo within the incoming magma at the level of the Pyroxenite Marker. If the pyroxene major element compositions were a product of incoming magma mixing with resident magma, one would expect a similar offset in

Downloaded from https://academic.oup.com/petrology/advance-article-abstract/doi/10.1093/petrology/egy081/5073045 by Rutgers University Libraries/Technical Services user on 02 October 2018

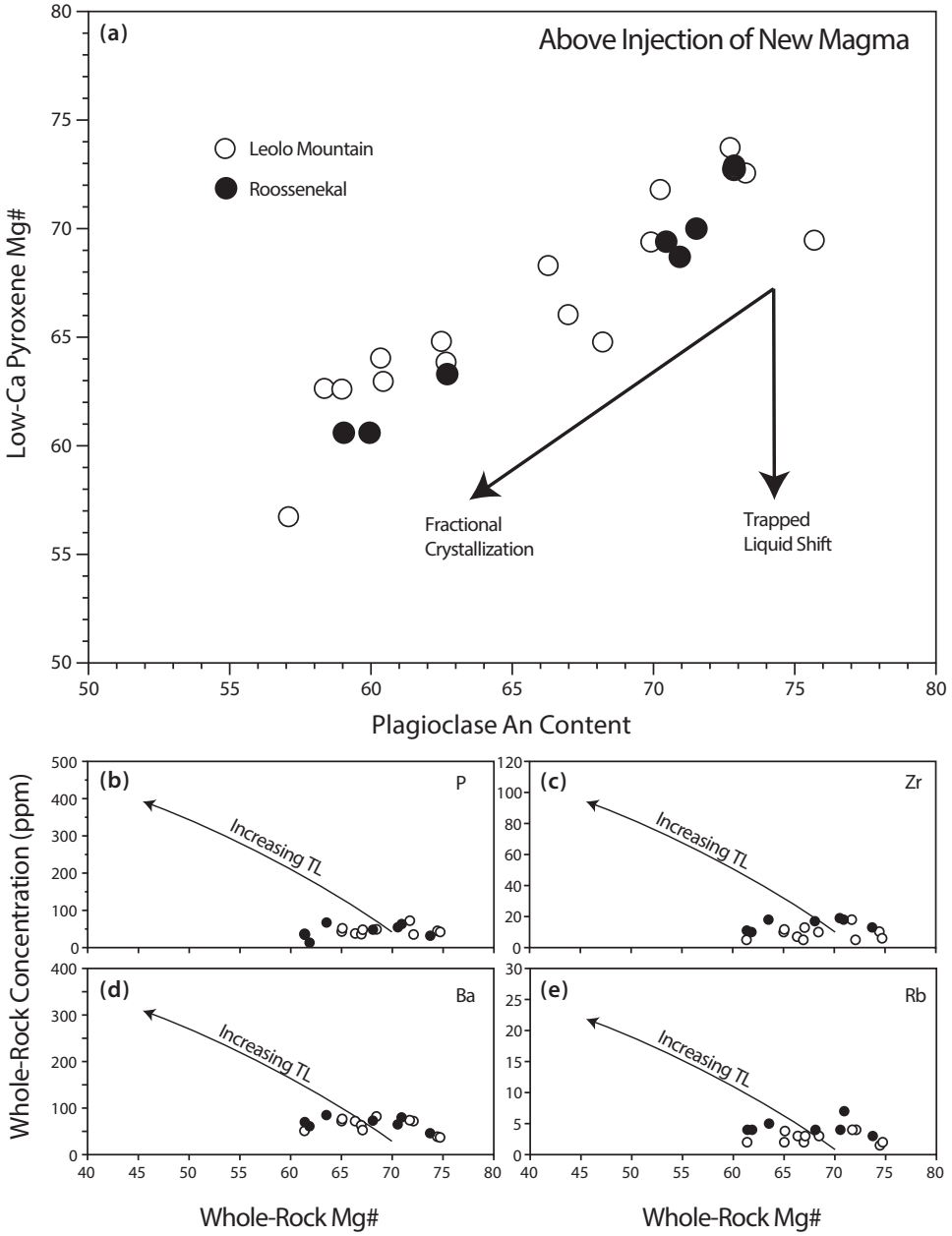

Fig. 13. (a) Average plagioclase core An content versus average low-Ca pyroxene core Mg#. (b–e) Whole-rock Mg# versus selected incompatible trace element concentrations (P, Zr, Ba, Rb) for both the Leolo Mountain and Roossenekal traverses. Only samples within, and immediately above, the Zone of Magma Mixing are shown. There is no noticeable difference between the two traverses above the input of new primitive magma, suggesting no increase in trapped liquid fraction within these samples from north (Leolo) to south (Roossenekal).

pyroxene Mg# between the two profiles throughout the Zone of Magma Mixing. Rather, it is likely that some fraction of the pyroxenes was intruded as a crystal cargo within the new incoming magma. This model is supported by the observation by Roelofse & Ashwal (2012) of isotopic disequilibrium between coexisting plagioclase and pyroxene within the lower Main Zone of the Northern Limb.

If a portion of the pyroxenes found in the Zone of Magma Mixing cumulates were entrained as a crystal cargo within the incoming magma, then the proposal of Cawthorn *et al.* (1991) that the incoming magma was denser than the resident magma must also be in question. The high Al_2O_3 of pyroxenes near the Pyroxenite Marker, as discussed by Cawthorn *et al.* (1991) as a signature of high-density liquid, would instead be explained by a higher pressure crystallization (e.g. Wood, 1974), as would be likely from a deeper staging chamber.

The intrusion of pyroxenes as a crystal cargo within the Zone of Magma Mixing inevitably leads to a questioning of the REE-in-plagioclase–clinopyroxene thermometer developed by Sun & Liang (2017). A fundamental assumption of the thermometer is that

Downloaded from https://academic.oup.com/petrology/advance-article-abstract/doi/10.1093/petrology/egy081/5073045 by Rutgers University Libraries/Technical Services user on 02 October 2018

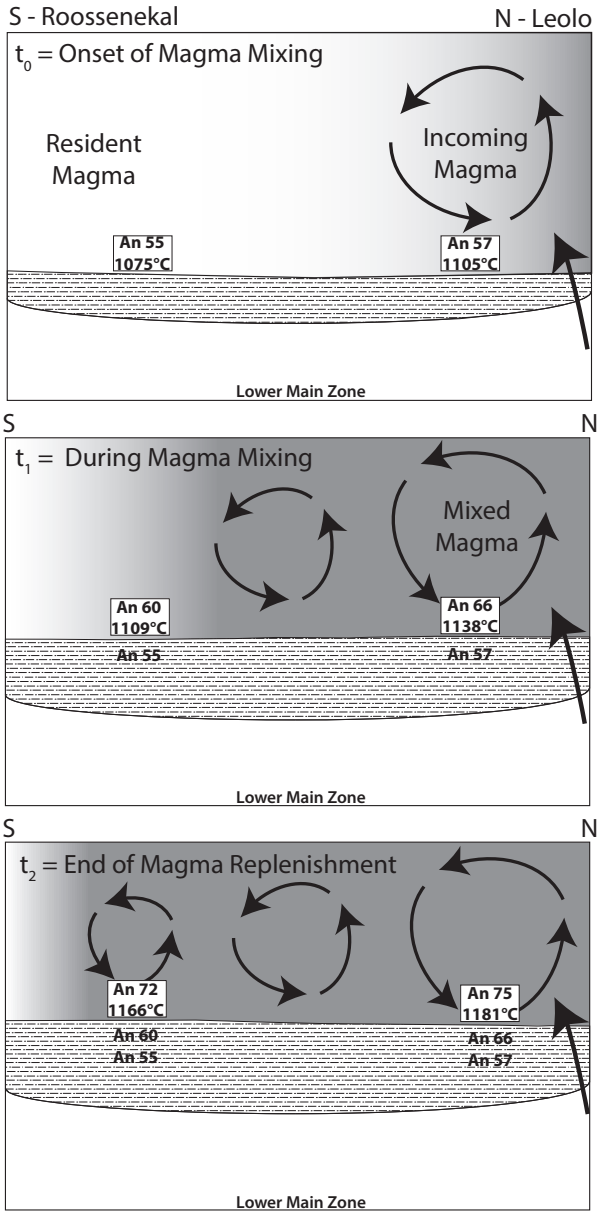

Fig. 14. Schematic illustration depicting the new emplacement model for the UUMZ. Stippled texture represents the cumulate pile. At t_0, new primitive magma is injected (represented by darker shading) in the northern part of the Eastern Limb and becomes fully mixed to the roof. The resident magma (represented by lighter shading), at the time of input, is crystallizing plagioclase of higher An content at higher temperatures in the north. The crystallization front at the chamber floor is evolving by *in situ* crystallization of a <4 m thick mush layer (e.g. Holness *et al.*, 2017). At t_1, incoming pulses of new primitive magma continue from the north while the mixed magma spreads to the south, with lower proportions of incoming versus resident magma from north to south. The resident magma at t_1 has more time to fractionate and crystallize, which, combined with the changing proportions of incoming magma, is reflected in the lateral changes in plagioclase An content and crystallization temperature. At t_2, magma replenishment ceases and the mixed magma has spread completely to the south, with decreasing proportions of incoming versus resident magma. Again, the resident magma in the south has had more time to fractionate and crystallize, resulting in lower plagioclase An content, crystallization temperatures and the more negative Eu anomaly recorded in the incoming magma composition at Roossenekal.

clinopyroxene and plagioclase were co-crystallized from the same parental magma, thus recording accurate crystallization temperatures of plagioclase. Sun & Liang (2017) conducted experiments testing the effectiveness of the thermometer in these types of situations by pairing plagioclase grains with random clinopyroxene grains that crystallized at various portions of a fractional crystallization sequence. Sun & Liang (2017) found that if the mineral pairs were both crystallized within a relative 10% crystallization sequence, this would ensure a discrepancy of $<10^{\circ}$C between REE-in-plagioclase–clinopyroxene calculated temperatures and temperatures calculated via plagioclase An content only. Sun & Liang (2017) tested the REE thermometer on 19 samples from the Leolo Mountain Traverse and compared the results with the An-based thermometer used by VanTongeren & Mathez (2013). VanTongeren & Mathez (2013) calculated crystallization temperatures assuming plagioclase of An_{75} crystallized at 1150°C and applied a slope of 6·8°C/An from MELTS modelling (Ghiorso & Sack, 1995; VanTongeren *et al.*, 2010). Based on new MELTS modelling, Sun & Liang (2017) updated the liquidus temperature of these samples to 1200°C and re-calculated the crystallization temperatures for the Leolo Mountain Traverse using the An-based thermometer. Sun & Liang (2017) note that there are REE patterns for the RLS gabbros that indicate plagioclase and clinopyroxene may have crystallized at different times; however, the REE calculated temperatures match closely with the An-based thermometer, demonstrating that the REE-in-plagioclase and clinopyroxene thermometer is providing reasonable plagioclase crystallization temperatures for the RLS Main Zone samples.

CONCLUSIONS

We present new data, including both major and trace element compositions of all mineral phases, to investigate the lateral variations associated with the replenishment of the Rustenburg Layered Suite at the level of the Pyroxenite Marker. The proportion of incoming versus resident magma below the Pyroxenite Marker decreases from north (Leolo) to south (Roossenekal). Crystallization temperatures recorded before magma addition, as well as near the Pyroxenite Marker, decrease from north to south. The calculated incoming magma composition at Roossenekal is elevated in incompatible element concentrations and depleted in compatible elements when compared with the incoming magma composition in the northern part of the Eastern Limb at Leolo, while also exhibiting a more prominent negative Eu anomaly. Reconstruction of the stratigraphic profile at Roossenekal using a shallow dip of 10° indicates that the input of new primitive magma, as well as the formation of the Pyroxenite Marker, occurs at approximately the same depth between the two profiles, suggesting that a structural basin (e.g. Cawthorn *et al.*, 2016) is not necessary to explain the lateral variations.

Downloaded from https://academic.oup.com/petrology/advance-article-abstract/doi/10.1093/petrology/egy081/5073045 by Rutgers University Libraries/Technical Services user on 02 October 2018

We conclude that new batches of primitive magma were periodically injected into the magma chamber and that the locus of magma injection in the Eastern Limb is near the Thabazimbi–Murchison Lineament (TML). The multiple small batches of new magma contained a pyroxene crystal cargo and mixed rapidly with the resident magma, while simultaneously crystallizing between pulses. The lateral variations are caused by a slightly enriched resident magma from north to south, a decrease in the proportion of incoming magma from north to south, and an incoming magma that is undergoing fractional crystallization.

Lateral variations ought to be considered in studies of the RLS and layered mafic intrusions in general. It is conceivable, as demonstrated here, that a directed input during magma recharge events can produce varying geochemical signatures observed over lateral distances at the same stratigraphic interval, potentially obfuscating the real magma chamber processes.

ACKNOWLEDGEMENTS

We thank J. Gross and T. C. Prissel for their assistance with electron microprobe analyses. We are also grateful to E. A. Mathez and N. A. Zirakparvar for assistance with field sampling and valuable discussions. We thank Freddie Roelofse, Christian Tegner and an anonymous reviewer for their comments and suggestions that improved this paper, as well as Jim Mungall for editorial guidance.

FUNDING

This work was supported NSF grant EAR-1624545 to J. VanTongeren.

SUPPLEMENTARY DATA

Supplementary data for this paper are available at *Journal of Petrology* online.

REFERENCES

Ashwal, L. D., Webb, S. J. & Knoper, M. W. (2005). Magmatic stratigraphy in the Bushveld Northern Lobe: continuous geophysical and mineralogical data from the 2950 m Bellevue drillcore. *South African Journal of Geology* **108**, 199–232.

Barnes, S. J. (1986). The distribution of chromium among orthopyroxene, spinel and silicate liquid at atmospheric pressure. *Geochimica et Cosmochimica Acta* **50**, 1889–1909.

Bédard, J. (2007). Trace element partitioning coefficients between silicate melts and orthopyroxene: parameterizations of *D* variations. *Chemical Geology* **244**, 263–303.

Bindeman, I. N., Davis, A. M. & Drake, M. J. (1998). Ion microprobe study of plagioclase–basalt partition experiments at natural concentration levels of trace elements. *Geochimica et Cosmochimica Acta* **62**, 1175–1193.

Buick, I. S., Maas, R. & Gibson, R. (2001). Precise U–Pb titanite age constraints on the emplacement of the Bushveld Complex, South Africa. *Journal of the Geological Society, London* **158**, 3–6.

Cameron, E. N. (1978). The lower zone of the eastern Bushveld Complex in the Olifants River trough. *Journal of Petrology* **19**, 437–462.

Cawthorn, R. & Webb, S. (2001). Connectivity between the western and eastern limbs of the Bushveld Complex. *Tectonophysics* **330**, 195–209.

Cawthorn, R. G. (2007). Cr and Sr: keys to parental magmas and processes in the Bushveld Complex, South Africa. *Lithos* **95**, 381–398.

Cawthorn, R. G., Meyer, P. S. & Kruger, F. J. (1991). Major addition of magma at the Pyroxenite Marker in the western Bushveld Complex, South Africa. *Journal of Petrology* **32**, 739–763.

Cawthorn, R. G., Lundgaard, K. L., Tegner, C. & Wilson, J. R. (2016). Lateral variations in plagioclase compositions, Main Zone, Bushveld Complex, South Africa: evidence for slow mixing of magmas in basinal structures. *Mineralogical Magazine* **80**, 213–225.

Charlier, B. & Grove, T. L. (2012). Experiments on liquid immiscibility along tholeiitic liquid lines of descent. *Contributions to Mineralogy and Petrology* **164**, 27–44.

Cherniak, D. (2003). Silicon self-diffusion in single-crystal natural quartz and feldspar. *Earth and Planetary Science Letters* **214**, 655–668.

Clarke, B., Uken, R. & Reinhardt, J. (2009). Structural and compositional constraints on the emplacement of the Bushveld Complex, South Africa. *Lithos* **111**, 21–36.

Dunn, T. & Sen, C. (1994). Mineral/matrix partition coefficients for orthopyroxene, plagioclase, and olivine in basaltic to andesitic systems: a combined analytical and experimental study. *Geochimica et Cosmochimica Acta* **58**, 717–733.

Eales, H. (2002). Caveats in defining the magmas parental to the mafic rocks of the Bushveld Complex, and the manner of their emplacement: review and commentary. *Mineralogical Magazine* **66**, 815–832.

Eriksson, P. & Altermann, W. (1998). An overview of the geology of the Transvaal Supergroup dolomites (South Africa). *Environmental Geology* **36**, 179–188.

Ghiorso, M. S. & Sack, R. O. (1995). Chemical mass transfer in magmatic processes IV. A revised and internally consistent thermodynamic model for the interpolation and extrapolation of liquid–solid equilibria in magmatic systems at elevated temperatures and pressures. *Contributions to Mineralogy and Petrology* **119**, 197–212.

Groeneveld, D. (1970). The structural features and the petrography of the Bushveld Complex in the vicinity of Stoffberg, eastern Transvaal. In: Visser, D. L. & von Gruenewaldt, G. (eds) *Symposium on the Bushveld Igneous Complex and Other Layered Intrusions* Johannesburg: Geological Society of South Africa, pp. 36–45.

Harney, D., Von Gruenewaldt, G. & Merkle, R. (1996). The use of plagioclase composition as an indicator of magmatic processes in the Upper Zone of the Bushveld Complex. *Mineralogy and Petrology* **56**, 91–103.

Hartzer, F. (1995). Transvaal Supergroup inliers: geology, tectonic development and relationship with the Bushveld Complex, South Africa. *Journal of African Earth Sciences* **21**, 521–547.

Holness, M. B., Cawthorn, R. G. & Roberts, J. (2017). The thickness of the crystal mush on the floor of the Bushveld magma chamber. *Contributions to Mineralogy and Petrology* **172**, 102.

Klemm, D., Ketterer, S., Reichhardt, F., Steindl, J. & Weber-Diefenbach, K. (1985). Implication of vertical and lateral compositional variations across the pyroxene marker and its associated rocks in the upper part of the Main Zone in the eastern Bushveld Complex. *Economic Geology* **80**, 1007–1015.

Downloaded from https://academic.oup.com/petrology/advance-article-abstract/doi/10.1093/petrology/egy081/5073045 by Rutgers University Libraries/Technical Services user on 02 October 2018

Kruger, F. (1991). Author's reply to discussion on the stratigraphy of the Bushveld Complex; a reappraisal and the relocation of the Main Zone boundaries. *South African Journal of Geology* **94**, 187–190.

Kruger, F. (1994). The Sr-isotopic stratigraphy of the western Bushveld Complex. *South African Journal of Geology* **97**, 393–398.

Kruger, F., Cawthorn, R. & Walsh, K. (1987). Strontium isotopic evidence against magma addition in the Upper Zone of the Bushveld Complex. *Earth and Planetary Science Letters* **84**, 51–58.

Kruger, F. J. (1990). The stratigraphy of the Bushveld Complex: a reappraisal and the relocation of the Main Zone boundaries. *South African Journal of Geology* **93**, 376–381.

Kruger, F. J. (2005). Filling the Bushveld Complex magma chamber: lateral expansion, roof and floor interaction, magmatic unconformities, and the formation of giant chromitite, PGE and Ti–V–magnetitite deposits. *Mineralium Deposita* **40**, 451–472.

Longridge, L., Gibson, R. L. & Nex, P. A. (2009). Structural controls on melt segregation and migration related to the formation of the diapiric Schwerin Fold in the contact aureole of the Bushveld Complex, South Africa. *Earth and Environmental Science Transactions of the Royal Society of Edinburgh* **100**, 61–76.

Lundgaard, K. L., Tegner, C., Cawthorn, R. G., Kruger, F. J. & Wilson, J. R. (2006). Trapped intercumulus liquid in the Main Zone of eastern Bushveld Complex, South Africa. *Contributions to Mineralogy and Petrology* **151**, 352–369.

McDonough, W. F. & Sun, S.-S. (1995). The composition of the Earth. *Chemical Geology* **120**, 223–253.

Mitchell, A. (1990). The stratigraphy, petrography and mineralogy of the Main Zone of the northwestern Bushveld Complex. *South African Journal of Geology* **93**, 818–831.

Mitchell, A. & Scoon, R. (1991). Discussion on 'The stratigraphy of the Bushveld Complex; a reappraisal and the relocation of the Main Zone boundaries'. *South African Journal of Geology* **94**, 183–187.

Molyneux, T. (1974). A geological investigation of the Bushveld Complex in Sekhukhuneland and part of the Steelpoort valley. *South African Journal of Geology* **77**, 329–338.

Molyneux, T. (2008). *Compilation on a Scale of 1: 50000 of the Geology of the Eastern Compartment of the Bushveld Complex. Special Publication 1 of the Johannes Willemse Bushveld Intelligence Centre*. Pretoria: Department of Geology, University of Pretoria.

Morse, S. (1984). Cation diffusion in plagioclase feldspar. *Science* **225**, 504–505.

Mungall, J. E., Kamo, S. L. & McQuade, S. (2016). U–Pb geochronology documents out-of-sequence emplacement of ultramafic layers in the Bushveld Igneous Complex of South Africa. *Nature Communications* **7**, 13385.

Nex, P., Cawthorn, R. & Kinnaird, J. (2002). Geochemical effects of magma addition: compositional reversals and decoupling of trends in the Main Zone of the western Bushveld Complex. *Mineralogical Magazine* **66**, 833–856.

Olsson, J., Söderlund, U., Klausen, M. & Ernst, R. (2010). U–Pb baddeleyite ages linking major Archean dyke swarms to volcanic-rift forming events in the Kaapvaal craton (South Africa), and a precise age for the Bushveld Complex. *Precambrian Research* **183**, 490–500.

Roelofse, F. & Ashwal, L. D. (2012). The Lower Main Zone in the Northern Limb of the Bushveld Complex—a >1.3 km thick sequence of intruded and variably contaminated crystal mushes. *Journal of Petrology* **53**, 1449–1476.

SACS. (1980). *Lithostratigraphy of the Republic of South Africa, South West Africa/Namibia and the Republic of Botswana, Transkei, and Venda*. South African Geological Survey Handbook **8**, 690 pp.

Scoates, J. S. & Friedman, R. M. (2008). Precise age of the platiniferous Merensky Reef, Bushveld Complex, South Africa, by the U–Pb zircon chemical abrasion ID-TIMS technique. *Economic Geology* **103**, 465–471.

Scoates, J. S. & Wall, C. J. (2015). Geochronology of layered intrusions. In: Charlier B., Namur O., Lapytov R., Tegner C. (eds) *Layered Intrusions*. Berlin: Springer, pp. 3–74.

Scoon, R. & Mitchell, A. (2012). The Upper Zone of the Bushveld Complex at Roossenekal, South Africa: geochemical stratigraphy and evidence of multiple episodes of magma replenishment. *South African Journal of Geology* **115**, 515–534.

Sharpe, B. (1982). Structures in Transvaal Sequence rocks within and adjacent to the eastern Bushveld Complex. *South African Journal of Geology* **85**, 29–41.

Sharpe, M. R. (1985). Strontium isotope evidence for preserved density stratification in the main zone of the Bushveld Complex, South Africa. *Nature* **316**, 119–126.

Sun, C. & Liang, Y. (2017). A REE-in-plagioclase–clinopyroxene thermometer for crustal rocks. *Contributions to Mineralogy and Petrology* **172**, 24.

Sun, S.-S. & McDonough, W-S. (1989). Chemical and isotopic systematics of oceanic basalts: implications for mantle composition and processes. In: Saunders, A. D. & Norry, M. J. (eds) *Magmatism in the Ocean Basins. Geological Society, London, Special Publications* **42**, 313–345.

Tanner, D., Mavrogenes, J. A., Arculus, R. J. & Jenner, F. E. (2014). Trace element stratigraphy of the Bellevue Core, Northern Bushveld: multiple magma injections obscured by diffusive processes. *Journal of Petrology* **55**, 859–882.

Uken, R. & Watkeys, M. K. (1997). Diapirism initiated by the Bushveld complex, South Africa. *Geology* **25**, 723–726.

VanTongeren, J. & Mathez, E. (2013). Incoming magma composition and style of recharge below the pyroxenite marker, eastern Bushveld complex, South Africa. *Journal of Petrology* **54**, 1585–1605.

VanTongeren, J. & Mathez, E. (2015). On the relationship between the Bushveld Complex and its felsic roof rocks, part 2: the immediate roof. *Contributions to Mineralogy and Petrology* **170**, 56.

VanTongeren, J. A. (2018). Mixing and Unmixing in the Bushveld Complex Magma Chamber. In: Mondal S. & Griffin W. L. (eds) *Processes and Ore Deposits of Ultramafic-Mafic Magmas through Space and Time*. Elsevier Inc, pp. 113–138.

VanTongeren, J. A., Mathez, E. A. & Kelemen, P. B. (2010). A felsic end to Bushveld differentiation. *Journal of Petrology* **51**, 1891–1912.

von Gruenewaldt, G. (1973). The main and upper zones of the Bushveld Complex in the Roossenekal area, eastern Transvaal. *Transactions of the Geological Society of South Africa* **76**, 207–227.

Webb, S. J., Cawthorn, R. G., Nguuri, T. & James, D. (2004). Gravity modeling of Bushveld Complex connectivity supported by Southern African seismic experiment results. *South African Journal of Geology* **107**, 207–218.

Wood, B. J. (1974). The solubility of alumina in orthopyroxene coexisting with garnet. *Contributions to Mineralogy and Petrology* **46**, 1–15.

Wood, B. J. & Blundy, J. D. (1997). A predictive model for rare earth element partitioning between clinopyroxene and anhydrous silicate melt. *Contributions to Mineralogy and Petrology* **129**, 166–181.

Zeh, A., Ovtcharova, M., Wilson, A. H. & Schaltegger, U. (2015). The Bushveld Complex was emplaced and cooled in less than one million years—results of zirconology, and geotectonic implications. *Earth and Planetary Science Letters* **418**, 103–114.

Downloaded from https://academic.oup.com/petrology/advance-article-abstract/doi/10.1093/petrology/egy081/5073045 by Rutgers University Libraries/Technical Services user on 02 October 2018